Contents lists available at ScienceDirect

Environmental Modelling and Software

journal homepage: www.elsevier.com

A generic data-driven technique for forecasting of reservoir inflow: Application for hydropower maximization

Shahryar Khalique Ahmad , Faisal Hossain *

Dept. of Civil and Environmental Engineering, Univ. of Washington, More Hall 201, Seattle, WA, 98195, USA

ARTICLE INFO

Keywords:
Reservoir inflow forecasting
Artificial neural network
Numerical weather prediction
Baseflow separation
Hydropower maximization
Global scalability

ABSTRACT

A generic and scalable scheme is proposed for forecasting reservoir inflow to optimize reservoir operations for hydropower maximization. Short-term weather forecasts and antecedent hydrological variables were inputs to a three-layered hydrologically-relevant Artificial Neural Network (ANN) to forecast inflow for 7-days of lead-time. Application of the scheme was demonstrated over 23 dams in U.S. with varying hydrological characteristics and climate regimes. Probabilistic forecast was also explored by feeding ANN with ensembles of weather forecast fields. Results suggest forecasting skill improves with decreasing coefficient of variation in inflow and increasing drainage area. Forecast-informed operations were simulated using a rolling horizon scheme and assessed against benchmark control rules. Over two years of operations from Pensacola dam (Oklahoma), additional 47,253 MWh of energy could have been harvested without compromising flood risk with optimal operations. This study reinforces the potential of a numerically efficient and skillful reservoir inflow forecasting scheme to address water-energy security challenges.

1. Introduction

Most of the world's artificial reservoirs are operated at daily or longer time scales based on rule curves that were designed using a climatology of historical flow observations and pre-dam storage volumes (Lee et al., 2009; Ficchì et al., 2015; Yazicigil et al., 1983). Rule curves outline the reservoir storage targets that need to be met at specific times of the year. Operating strictly based on these climatology-based rules can lead to mishandling of an unexpected peak reservoir inflow event (Miao et al., 2016). For instance, in a relatively dry flood season, lowering the pool to rule curve level can result in significant loss in hydropower generation, which could be avoided if weather forecasts were made ahead of time.

For efficient operations of a single/multipurpose reservoir system, the information about forecast inflow into the system is an important part of the real-time decision-making process. Short-term daily to weekly scale forecasts are indispensable in maximizing societally important benefits of flood control and hydropower generation (Yazicigil et al., 1983; Anghileri et al., 2016). Flood mitigation requires sufficient flood storage before an impending flood, while hydropower generation requires maximizing the economic value of water by releasing most of it through turbines and keeping reservoir at maximum pool. Reservoir inflow forecasts, if reasonably skillful, can help achieve a balance where hydropower can be maximized without compromising flood risk downstream (Jordan et al., 2012; Madsen et al., 2009; Qi et al., 2017). Often, this is achieved by proactive storage or release from reservoir in anticipation of reservoir inflow. Recently, a study on two dams in US showed application of Numerical Weather Prediction model (NWP)-based reservoir inflow forecasts for optimizing the reservoir operations (Ahmad et al., 2018). Significant hydropower benefits were demonstrated without compromising the flood control objective. Ongoing projects such as Integrated Forecast and Reservoir Management (INFORM) (Georgakakos et al., 2007) and Forecast Informed Reservoir Operations (FIRO Overview, 2017), focused over specific watersheds, are also utilizing short-term weather forecasts for operating the reservoirs.

The NWP models from various meteorological agencies produce weather-scale forecast fields of temperatures, wind, precipitation, soil moisture in three dimensions over the entire globe. These publicly available forecasts represent an underutilized resource for the hydropower community, due to concern over fossil-fuel based environmental degradation (Dudhani et al., 2006; Li, 2005). Moreover, efficient management of hydropower facilities is essential for emerging

* Corresponding author.
Email address: fhossain@uw.edu (F. Hossain)

https://doi.org/10.1016/j.envsoft.2019.06.008
Received 5 March 2019; Received in revised form 18 June 2019; Accepted 20 June 2019
Available online xxx
1364-8152/

economies where demand for energy often exceeds supply or generation capacity (Asif and Muneer, 2007). As more hydropower dams are constructed, especially in developing nations, achieving the highest possible operational efficiency using available weather forecasts can address the growing resource needs of today. The challenge today is to convert the global and public availability of weather forecasts to locally actionable data as reservoir inflow forecast, and thus mainstream their use in the operational world.

However, there are logistic hurdles to globalizing hydropower maximization techniques based on NWP-based reservoir inflow forecasts. Even if the forecasts achieve certain level of accuracy, adequate computational resources are required to capture sudden peak flow events considerably faster than real-time. This is because at a global scale, the NWP models lack sufficient detail to force hydrological models over the reservoir catchments where precipitation can often exhibit higher spatial variability (Flint and Flint, 2012; Do Hoai et al., 2011). Dynamic downscaling techniques have subsequently emerged in recent past that are known to be locally constrained rendition of weather forecasts at hydrologically relevant scale (Wilby and Wigley, 1997). However, dynamic downscaling is computationally intensive and not feasible for computationally-constrained settings of most operational reservoir management agencies around the world. For example, a study on flood forecasting in Houston, TX found that it takes nearly 7–20 h for dynamically downscaling of NWP forecasts for 24-hr lead-time depending on the configuration of CPU available in the current market (Sikder et al., 2019).

In summary, there are two important hurdles for operationalization of reservoir inflow forecasts in real-time reservoir optimization models around the world. These are: 1) uncertainty in inflow forecast (Zhao et al., 2011; Georgakakos et al., 2008; Faber and Stedinger, 2001), and 2) computational burden of deriving these reservoir inflow forecasts (Cheng et al., 2014).

For large-scale applications of NWP forecast fields in optimizing reservoir operations for hydropower maximization, an alternate and scalable numerical scheme is required. Such a scheme should have the following desired properties: 1) it has to be numerically efficient and considerably faster than real-time for practical operations; 2) it has to allow rapid multi-year historical assessment to understand risks of false positives and negatives in operations; 3) it has to be effective in limited in-situ hydrologic data settings for application in developing countries; and 4) it has to be skillful and yield physically realistic forecasts for streamflow over the forecast horizon.

Our selected scheme that we present here with such desired features is the data-based technique of Artificial Neural Networks (ANN) tailored for reservoir inflow forecasting. The ANN technique, over the last two decades, has proven to be an efficient supplement to modeling qualitative and quantitative water resource variables and capturing the nonlinearity in flow (Maier et al., 2010; Jain et al., 2009; Maier and Dandy, 1996; Hutton and Kapelan, 2015; Wei, 2016; Govindaraju and Rao, 2000; Wu et al., 2014). As noted by ASCE Task Committee on Application of ANNs in Hydrology (2000), ANNs are robust tools for many of the complex hydrological modeling problems. The review of relevant research on ANNs by Maier et al. (2010) suggest that a vast majority of studies have focused on flow prediction. Daily short-term flow forecasting using ANN has been explored, amongst others, by Birikundavyi et al. (2002), Kişi (2005), Wu et al. (2009), Coulibaly et al. (2000) and Zemzami et al. (2016). As required in all modeling efforts, following good practice that increases the credibility and impact of modeling results (Jakeman et al., 2006; Welsh, 2008), is particularly important for ANN models that are developed using available data and not explicitly based on underlying physical processes. For the input nodes, past conditions of streamflow and hydro-meteorological variables are commonly used in predicting future flow. Studies also used other predictor combinations such as flow length and travel time (Akhtar et al., 2009), previous day's rainfall and temperature (Lorrai and Sechi, 1995), flow, rainfall and evapotranspiration (Anctil et al., 2004), soil moisture deficits and runoff (Cheng and Noguchi, 1996). Bartoletti et al. (2018) eliminated the redundancy in antecedent rainfall using the data-driven Principal Component Analysis technique. However, to the best of our knowledge, there is no work on the use of freely available global NWP weather forecasts as ANN inputs.

Several studies using only the antecedent conditions have indicated the inability of ANN to capture the flow peaks (e.g., Campolo et al., 1999; Sudheer et al., 2003; Wu et al., 2009; De Vos and Reintjes, 2005). To provide an accurate estimate of peaks, it is necessary to remove the local variations caused by extreme flows from the time series function being mapped. Streamflow transformation is used to simplify the data structure following a convenient statistical model (Sudheer et al., 2003). As found by Zemzami et al. (2016), separation of streamflow into baseflow and runoff components improved the peak flow estimation and hence, it was incorporated in the present research. The runoff component was transformed by a moving average procedure to improve the peak flow prediction. Further, studies on ANN-based reservoir inflow prediction have primarily focused over only a specific reservoir system. In an effort to demonstrate global scalability, application of any proposed inflow forecasting scheme extending over multiple dams with varying hydro-climatic and geographic characteristics is necessary.

The innovative aspects of this study include development of ANN model based on the coarser scale forecast fields of 1–7 days lead from NWP weather models to predict basin-scale hydrology. The technique was tested over an inventory of 23 dams with widely varying hydrological characteristics and local climate regimes. A comprehensive validation framework was employed to assess the skillful and physical realism of the modeled forecasts. The probabilistic nature of inflow forecasts was addressed by obtaining an ensemble of forecast flow derived from ensemble of weather forecast. The forecasts were further incorporated in a reservoir optimization model for maximizing the daily hydropower generation while meeting other dam management constraints and regulations. The specific research questions of this study are: (1) *Can the use of ANN with pertinent hydrologic knowledge be computationally efficient, skillful and globally scalable in forecasting the reservoir inflow over short term forecast horizon (1–7 days)?* (2) *What role does the hydrological characteristics of the upstream basin and local climate zone play in driving the forecast skill of the designed ANN model?* (3) *Can such fast inflow forecasts be used to optimize the reservoir operations to improve energy generation without compromising flood or dam safety?*

The rest of the paper is organized as follows. In the next section we discuss the selection of dam sites for application of the proposed technique, followed by a description of datasets used. This is then followed by a detailed methodology and different components involved in Section 3. The case study results of ANN-based forecasts over the database of dams and its application for optimization of reservoir operations are presented in Section 4, followed by discussion and concluding remarks in Section 5.

2. Study sites and hydrometeorological data

In order to address the first two research questions, 23 dams located in various climate zones of the contiguous U.S. (CONUS) were selected. All selected dams receive unregulated flow and are operated for a variety of purposes such as flood control, hydropower generation, water supply, irrigation and recreation. Fifteen of these dams are powered. The dam inventory also represents a wide range of upstream catchment area, topography, hydrological characteristics, flow patterns, reservoir storage and installed hydropower capacity. The dams are shown in Fig. 1 by location and size of upstream drainage area. Apart from the study sites within US, six dam sites in large river basins of Ganges, Brahmaputra and Mekong were identified. Table 1 presents the information about the selected study sites with descriptive statistics of the original flow data over 2007–2014.

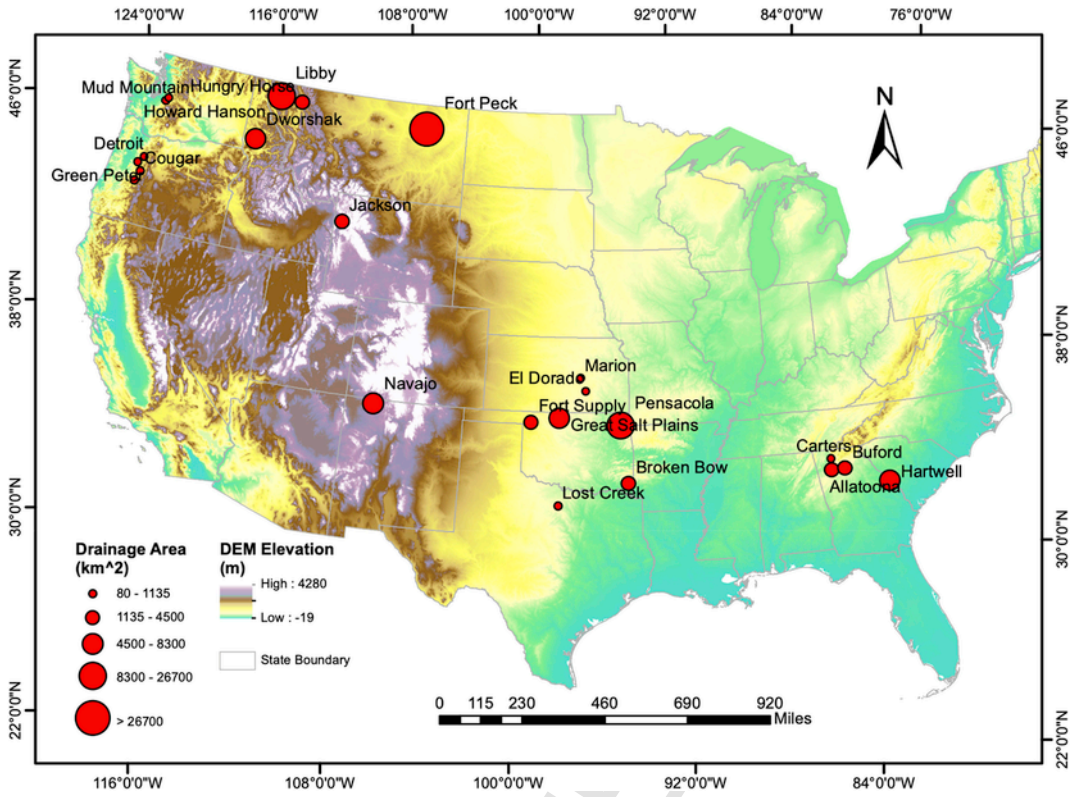

Fig. 1. Selected inventory of 23 dams, receiving mostly unregulated flow, for application of ANN-based inflow forecasting. The markers are sized by the area of upstream drainage basin.

Table 1
Selected study dams (in CONUS) and stations (on river basins in Asia) for application of ANN based flow forecasting technique with descriptive statistics of the basin/flow.

#	Dam/Station Name	Mean Flow (cfs)	Std. Dev of Flow (cfs)	COV	Drainage Area (km^2)	Reservoir Storage (km^3)	Koppen Climate Class	State/Basin
1	Allatoona	1447.33	2214.58	1.53	2893	0.83	humid subtrp	GA
2	Broken Bow	1375.51	3597.79	2.62	1995	1.98	humid subtrp	OK
3	Buford	1714.45	2238.86	1.31	2694	3.15	humid subtrp.	GA
4	Carters	562.86	649.33	1.15	966	0.58	humid subtrp	GA
5	Cougar	933.91	850.65	0.91	544	0.27	mediterranean	OR
6	Detroit	2207.62	2052.71	0.93	1134	0.56	mediterranean	OR
7	Dworshak	5731.71	6543.91	1.14	6320	4.39	cold dry	ID
8	Eldorado	191.45	757.38	3.96	606	0.30	cold humid	KS
9	Fort Peck	10282.50	9562.12	0.93	149508	23.56	semi-arid	MT
10	Fort Supply	43.11	103.68	2.41	4978	0.12	humid subtrp.	OK
11	Great Salt	413.68	1142.63	2.76	717	1.22	humid subtrp.	OK
12	Green Peter	1572.91	2122.20	1.35	8288	0.53	mediterranean	OR
13	Hartwell	3150.38	3601.98	1.14	5408	4.24	humid subtrp.	GA
14	Hills Creek	1198.80	1134.96	0.95	1008	0.44	mediterranean	OR
15	Howard	1070.65	1297.74	1.21	572	0.17	cold humid	WA
16	Hungry Horse	3949.58	5624.46	1.42	4248	3.68	cold humid	MT
17	Jackson	1478.85	2072.66	1.40	2134	1.08	cold humid	WY
18	Libby	12252.60	15028.93	1.23	23403	7.43	cold humid	MT
19	Lost Creek	1861.67	1034.76	0.56	88	0.03	humid subtrp.	TX
20	Marion	93.28	389.11	4.17	518	0.23	cold humid	KS
21	Mud Mountain	1653.07	1289.34	0.78	1036	0.13	temperate	WA
22	Navajo	1017.90	1112.65	1.09	8262	1.28	cold humid	NM
23	Pensacola	8669.14	15613.03	1.80	26672	2.71	humid subtrp.	OK
Large Basin Stations:								
1	Hardinge Bridge	9739.14	12406.50	1.27	985259	–	humid subtrp.	Ganges
2	Bahadurabad	17787.32	16055.54	0.90	525349	–	tropical/humid subtrp.	Brahma-putra
3	Vientiane	3951.18	3350.90	0.85	90469	–	tropical	Mekong
4	Pakse	9670.50	9399.63	0.97	349928	–	tropical	Mekong
5	Stung Treng	13663.62	13061.23	0.96	445074	–	tropical	Mekong
6	Kampong. Cham	14882.85	15374.09	1.03	470737	–	tropical	Mekong

Data for this study over the CONUS are as follows: (a) deterministic and ensemble forecast hydro-meteorological forcing fields, (b) basin's antecedent conditions, and (c) current reservoir state. The deterministic forecast fields of precipitation, temperature and windspeed were acquired from the Global Forecast System (GFS) global-scale Numerical Weather Prediction model at 0.5° resolution for 1–7 days lead-time with a 3-hourly temporal resolution. The archived data is available from Oct 2006, due to which the period of analysis in this study was

set to 2007–2017 and all the other datasets were gathered over this period. For the ensemble forecast fields, NOAA's Global Ensemble Forecasting System Reforecast (version 2) dataset (GEFS/R) (Hamill et al., 2013) with 11-member ensemble of forecasts at 1° resolution was used. The antecedent precipitation over the basin was obtained from the Climate Hazards Group InfraRed Precipitation with Station data (CHIRPS) gridded rainfall time series at 0.05° resolution (Funk et al., 2015), antecedent temperature and windspeed from in-situ Global Surface Summary of the Day (GSOD) data (Global Surface Summary of the Day, 2018) and antecedent soil moisture from Global Land Data Assimilation Systems (GLDAS). All the gridded datasets were processed to calculate the basin-averaged values to be used as inputs to ANN. The antecedent observed reservoir inflow for US dams was obtained from the dam operating agencies of US Army Corps of Engineers (USACE) and US Bureau of Reclamation (USBR). State of current reservoir storage and headwater level was acquired from the respective agencies' data portals. The climate zones for each dam were extracted from Köppen-Geiger climate classification (Peel et al., 2007). For the real-time forecasting and reservoir operation purpose, a forecast horizon of 1–7 days ahead was chosen.

3. Methodology

The experimental approach followed in the study is shown in Fig. 2 and described in the following sections.

3.1. Proposed ANN architecture

The ANN architecture used here is the multilayer feedforward neural network. This is one of the most popular architecture used for streamflow forecasting (Wu et al., 2009). It involves input, hidden and output layers where the hidden layer allows the network to perform complex nonlinear mapping between the input and output variables (Coulibaly et al., 2000; Funhashi et al., 1989). A three-layered ANN with one hidden layer was implemented. Many experiments in the past have confirmed this to be adequate for most forecasting problems (Lippmann, 1987; Zhang et al., 1998; Coulibaly et al., 2000). The network's ability to learn from training data and generalize depends on the number of nodes in input and hidden layers.

The sum of the weighted nodes of a layer form input to a transfer function that determines the output of that node. Nonlinear functions allow the network to learn nonlinear relationships between input and output vectors. The S-shaped log sigmoidal function was employed that acts as a squashing function bounding the output between zero and one and is the most commonly used for hidden layer nodes (Zealand et al., 1999). The output y_j from the j^{th} neuron of the layer is:

$$y_j = \frac{1}{1 + e^{-\left(\Sigma w_{ji} x_i\right)}} \tag{1}$$

where, w_{ji} = weight of the connection joining the j^{th} neuron in a layer with i^{th} neuron in the previous layer, and x_i = value of the i^{th} neuron in the previous layer. The linear function, as recommended for the nonlinear regression problems, was used for the output node activation.

3.2. ANN input predictors

Selection of input nodes for developing an ANN model is a difficult task that needs attention and a good understanding of the underlying physical processes. Relying solely on the model to identify critical inputs from a large subset can lead to misconvergence, poor accuracy and curse of dimensionality (Bowden et al., 2005). Sudheer et al. (2002) proposed a better alternative to the popular trial-and-error approach, utilizing the statistical properties (cross-, auto- and partial auto-correlation) of the observed data series for identifying appropriate input vector to the network.

The candidates for the input layer nodes for the proposed ANN scheme were: (1) NWP forecasts of precipitation, temperature and windspeed, obtained from the GFS model, produced at 0.5° resolution; (2) antecedent precipitation over the basin, (3) antecedent streamflow into the reservoir; and (4) antecedent baseflow. The gridded hydrometeorological inputs were obtained as daily basin-averaged values over the dam's upstream catchment area. The flow series can be viewed as the sum of baseflow and runoff signals, which when selected adequately as ANN inputs can improve model performance (Zemzami et al., 2016). The baseflow was separated from the daily observed reservoir inflow using the Recursive Digital Filter (RDF). RDF has been shown to perform better than other filtering techniques (Corzo et al., 2007; Zemzami et al., 2016). The general form of the filter is:

$$b_k = \frac{\left[\left(1 - BFI_{max}\right) \cdot a \cdot b_{k-1} + (1 - a) \cdot BFI_{max} \cdot y_k\right]}{1 - a \cdot BFI_{max}} \tag{3}$$

$$r_k = y_k - b_k \tag{4}$$

where, y_k is the total streamflow, b_k is the separated baseflow and r_k is runoff component at time k. It involves two filter parameters that need prior calibration: a, the recession constant and BFI_{max}, the maximum value of the baseflow index that can be modeled by the algorithm (Eckhardt et al., 2005). The initial baseflow, b_0 is also an unknown (assumed zero in this study for simplicity).

The runoff signal exhibits high local variations due to varying skewness in the data series especially for the smaller drainage areas. This can lead to underestimation of peak flow. An appropriate data transformation is needed to reduce these variations and improve the performance (Sudheer et al., 2003). The moving average method was used here that is also found to improve the time lag in modeled peaks flows (De Vos and Reintjes, 2005). The moving average smoothens flow time series by replacing each data point with the average of previous K data points, K being the length of the memory window, with same weight applied to each data point. Instead of the antecedent runoff time series, the moving average over total streamflow was applied to obtain the in-

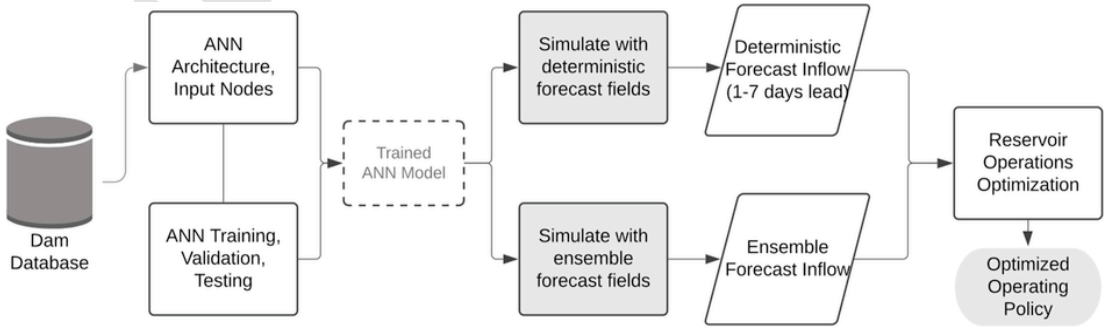

Fig. 2. Experimental approach showing development and testing of ANN architecture, and its integration with the reservoir operations optimization to achieve hydropower maximization.

put node. Once the candidate predictors were identified, the statistical properties of cross- and partial autocorrelation between the predictors and the streamflow were used for finding the optimal number of antecedent days for each variable. The number of hidden layers in the architecture and the baseflow parameters were selected using a trial-and-error procedure. With this configuration, a sensitivity analysis was performed where ANN was trained with different combinations of antecedent/forecast predictors to select the best combination of input predictors for the study sites. This procedure for input predictor selection is schematically shown in Fig. 3.

3.3. ANN training algorithm

The training of an ANN, or determining the weights of the ANN nodes, was performed using a learning algorithm to minimize an error function by providing input-output examples (training data). As found by several studies, the Levenberg-Marquardt (LM) training method is the most effective method for feed-forward neural networks with respect to the training precision (Liu, 2010; Kişi, 2007; Sun et al., 2016; Anctil et al., 2004). The algorithm blends the stability of steepest descent method and the speed advantage of Gauss–Newton algorithm providing a robust way to find the optimal weights, without having to compute the Hessian matrix (Moré, 1978). The MATLAB implementation of LM training in the Neural Network Toolbox was used here (The Mathworks Inc., Natick, Massachusetts).

The most critical issue in training a multi-layer ANN is its ability to generalize the modeled outputs. While an overly complex ANN structure can potentially fit the noise in the training data leading to the overfitting, an insufficient level of complexity can result in lack of generalization ability that fails to detect regularities in the data set, which is also known as underfitting (Coulibaly et al., 2000). To avoid these issues, the early stopped training approach (STA) is incorporated within the LM training. The STA involves dividing the entire data into three subsets – (i) a *training set,* which is used to compute the gradient and update the weights and biases of the network, (ii) *validation set* over which the errors are monitored during the training process and is used to decided when to stop training, (iii) *test set,* which is not used in the training process but is used to assess the expected performance in the future. During the initial phase of training, the training and validation set errors decrease. However, when the network begins to overfit the data, the error on the validation set typically begins to rise. When the validation error increases for a specified number of iterations, the training is stopped, and the weights and biases at the minimum of the validation error are returned. This threshold number of iterations is chosen to be six in this study. As recommended by Maier and Dandy (2000), this threshold avoids any utilization of validation/test set data during the training process, either to optimize the network inputs and parameters or to decide when to stop training.

Another method to improve the generalization, called regularization was used that modifies the performance function for training. The procedure adds a term to the performance function consisting of the mean of the sum of squares of the network weights and biases. This causes the network to have smaller weights and biases and forces the network response to be smoother and less likely to overfit. The performance ratio of 0.5, which gives equal weight to the mean square errors and the mean square weights was chosen.

The daily inflow forecast over 7-day horizon was obtained using an iterative multi-step forecasting method. The ANN modeled flows at the first lead-time are used as the antecedent flow conditions for the next step's model input, including all other past information. With each subsequent lead-time, ANN's own outputs are used iteratively to model the 7-day ahead forecasts. The metrics used for assessing the ANN performance include Nash Sutcliffe Efficiency (NSE), Root Mean Square Error (RMSE), Correlation (R^2) and Mean Absolute Error (MAE).

3.4. Forecast performance assessment

To ensure that the trained ANN model does not contain known or detectable flaws and can be used with confidence over any unseen data, a comprehensive assessment was performed using different facets of the modeled ANN flow. Specifically, three aspects of the model validity are considered here, namely (a) *replicative validity*: how well the ANN model can capture the general underlying relationship in the calibration data (b) *predictive validity*: the ability of the model to generalize or learn the specific patterns in the calibration data, (c) *structural validity*: plausibility of the model when compared with a priori knowledge (Humphrey et al., 2017). For, the replicative validity, the model fit is evaluated, and residuals are analyzed for violation of error model assumptions using graphical plots of predictions and residuals. The predictive validity is ensured by demonstrating the model's performance on an independent test set in addition to the training and cross-validation sets such that there is no overfitting and underfitting. Lastly, for structural validity, the relative contribution of each input predictor to the model output is assessed using a sensitivity analysis (described in section 4.1). The more complex methods to quantify relative importance of inputs found in literature are skipped here as replicative and predictive validity are most important for forecasting problems. For further details, the reader is referred to Humphrey et al. (2017) who proposed such a validation framework for multilayer ANNs.

3.5. ANN-based forecasts for reservoir operations optimization

The inclusion of forecast variables as a part of ANN input predictor set allows for using different forecast products to model the forecast flow. The trained ANN model when fed with the GFS and GEFS-based deterministic and ensemble forecast fields, respectively, over the test period results in deterministic and ensemble members of forecast for 1–7 days lead time. The forecast flow was used to optimize the release decisions to maximize the hydropower generation, without compromising the flood control and dam safety. The focus in this study is on dams that overwhelmingly require daily or longer time horizon for decision-making. Hence, the optimization was set up with daily temporal scale

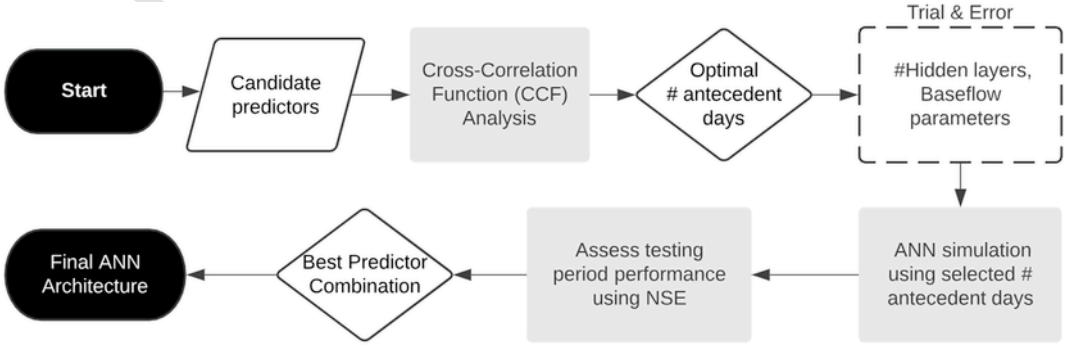

Fig. 3. A schematic of different steps involved in building the ANN architecture and input predictor combination.

over a horizon of 1–7 days. The study formulates the following two operating schemes to demonstrate the application and value of forecast flows in reservoir operations.

3.5.1. Forecast-guided operations using model predictive control scheme

This scheme is devised to simulate the reservoir operations using short-term deterministic forecasts over 1–7 days lead-times to generate daily release decisions that are optimal according to a constrained objective function. The release at first time step was implemented while the later ones were revised at the next step's model run using updated forecasts. Such a strategy termed as Model Predictive Control (MPC) (or 'rolling horizon'), was proposed by Mayne et al. (2000) and implemented by Turner et al. (2017). The objective in this study was set to minimize the hydropower deficit from maximum installed capacity (or, to maximize energy generated) over the forecast horizon based on the optimized releases. The end-state of reservoir at the end of 7th day is controlled using a penalty function that considers the reservoir state beyond the forecast horizon. This penalty function was proportional to the amount of deviation of the terminal reservoir level from the rule curve specified level. During the flood seasons, excessive spillway release was kept in check to minimize potential downstream damage. If a flood event is forecasted causing the reservoir level to reach the flood storage pool, the penalty function was modified to the sum of spillway release from the reservoir over the 7-day period. Thus, the selected penalty function grants preference to those release decisions that either minimize large deviations from rule curve specified levels or minimize the downstream flood risk, based on the season of reservoir operation.

The major objective of energy maximization and the penalty function were implemented in the form of a Multi-objective Optimization Problem (MOP) seeking Pareto optimal set of solutions (Madsen et al., 2009). The suitability of Pareto optimal solutions for MOPs in reservoir operations has been demonstrated, amongst others, by Chen et al. (2017), Yang et al. (2015) and Giuliani et al. (2016). The Non-dominated Sorting Genetic Algorithm (NSGA-II; Deb et al., 2002) was used to yield the Pareto front of the optimal solutions, where none of the objective functions can be improved further without violating the other.

Several constraints were imposed for optimizing the reservoir releases in the interest of downstream stakeholders, dam safety and environmental concerts. Logistical constraints included turbine and spillway capacity limiting the power and spillway release and storage-volume continuity. The minimum reservoir storage was set to 95% of the historical minimum while limited by the flood control pool. The flood control constraint was implemented by limiting the total release to a safe threshold considering downstream flooding. The environmental flow was used to set the minimum release. The mathematical formulation and details of the constraints and objective functions are given in Appendix B.

3.5.2. Benchmark scheme

To assess the performance and value of optimizing the reservoir operations using the flow forecasts, a benchmark operating scheme is needed. In reality, dam operations would take into account many other factors that cannot be easily accommodated in a scientific analysis including regulatory requirements, power grid requests for hydropower dispatch, and recreation demands from local agencies. Thus, the hydropower benefits cannot be directly compared against the respective benefits from actually observed operations. Hence, a customized operation scheme was designed targeted specifically at maximizing the hydropower objective function (Turner et al., 2017). As proposed by Turner et al. (2017), the control rules were designed in the form of look-up table where the optimal release is specified as a function of two state variables – the reservoir storage level and season of year. We followed here the most rigorous way of designing such rules by optimizing the operations using the observed time series data over 24 years from 1995 to 2018. The objective function was to maximize the total energy generated by the reservoir (which is the same objective as used for the optimization based on the forecasts). Although, the forecast-guided operations were obtained using daily optimization, a monthly time step was chosen to obtain the control release policy for benchmarking considering the huge number of data points to optimize over at daily scale.

3.6. ANN-based ensemble forecasting

The inherent uncertainty in the forecast variables of precipitation and temperature from the NWP models propagate in the modeled flow forecasts. To account for this uncertainty in modeled flow, the input predictors of forecast precipitation and minimum and maximum temperature from the ensemble forecast product of GEFS were inputs to the selected ANN configuration. Corresponding to each of the 11 GEFS ensemble members, 11 different realizations of the 1–7 days lead time forecast flow were obtained from the ANN model. The numerically fast ANN technique allowed the simulation of all the ensemble members in minimal processing time.

Next, the optimization model, set up to use deterministic forecasts, was simulated with three scenarios of GEFS-based forecast flow – the minimum, maximum and average of the ensemble inflow members. Maximizing the objective function value across all ensemble members to optimize decisions will undermine the dam operator's ability to adjust release in response to new information (Turner et al., 2017). The use of multi-stage stochastic optimization for optimization based on ensemble forecasts can also be found in literature (Xu et al., 2015; Fan et al., 2016). However, due to its computationally demanding requirements and complex implementation, we have limited the study here with a deterministic rolling horizon type optimization for probabilistic forecast using minimum, maximum and average of the ensemble scenarios.

4. Results from case studies

The ANN based forecasting was tested for each of the 23 selected dam sites and the performance was assessed individually. The ensemble forecasting was applied to 3 dams for demonstrating the concept and performance. Finally, the reservoir operations optimization using the modeled forecasts is shown for a single dam. The detailed results are described in the following sections.

4.1. ANN architecture and input selection

For arriving at the optimal input combination, first the number of antecedent days for the candidate predictor variables, as identified in section 3.2, was determined using the statistical properties of the respective time series. We chose to perform this analysis first for one of the dams – Pensacola dam (located in Oklahoma, USA) to obtain an estimate of probable predictors and then tested the configuration for other dams.

The cross-correlation function (CCF), measuring the similarity of a time series with the lagged versions of another, was obtained for the antecedent variables of precipitation, baseflow, temperature, windspeed, against the observed streamflow series at various lags. Partial autocorrelation of observed streamflow was plotted to assess the predictability in the antecedent flow. As shown in Fig. 4(a), the cross-correlations decay with increased lags and are significantly high for precipitation and baseflow for use as predictors for ANN. The streamflow PACF indicates significant correlation up to lag 3 and falls sharply thereafter below the confidence limits. For the moving averaged streamflow as input, the best value of memory window length$K$, was determined using the cross-correlation between streamflow and antecedent moving-averaged flow as plotted in Fig. 4(b) for K values of 3, 5 and 8 for the Pensacola dam. From the CCF plots, it can be observed that the moving average flow correlates differently at different lags

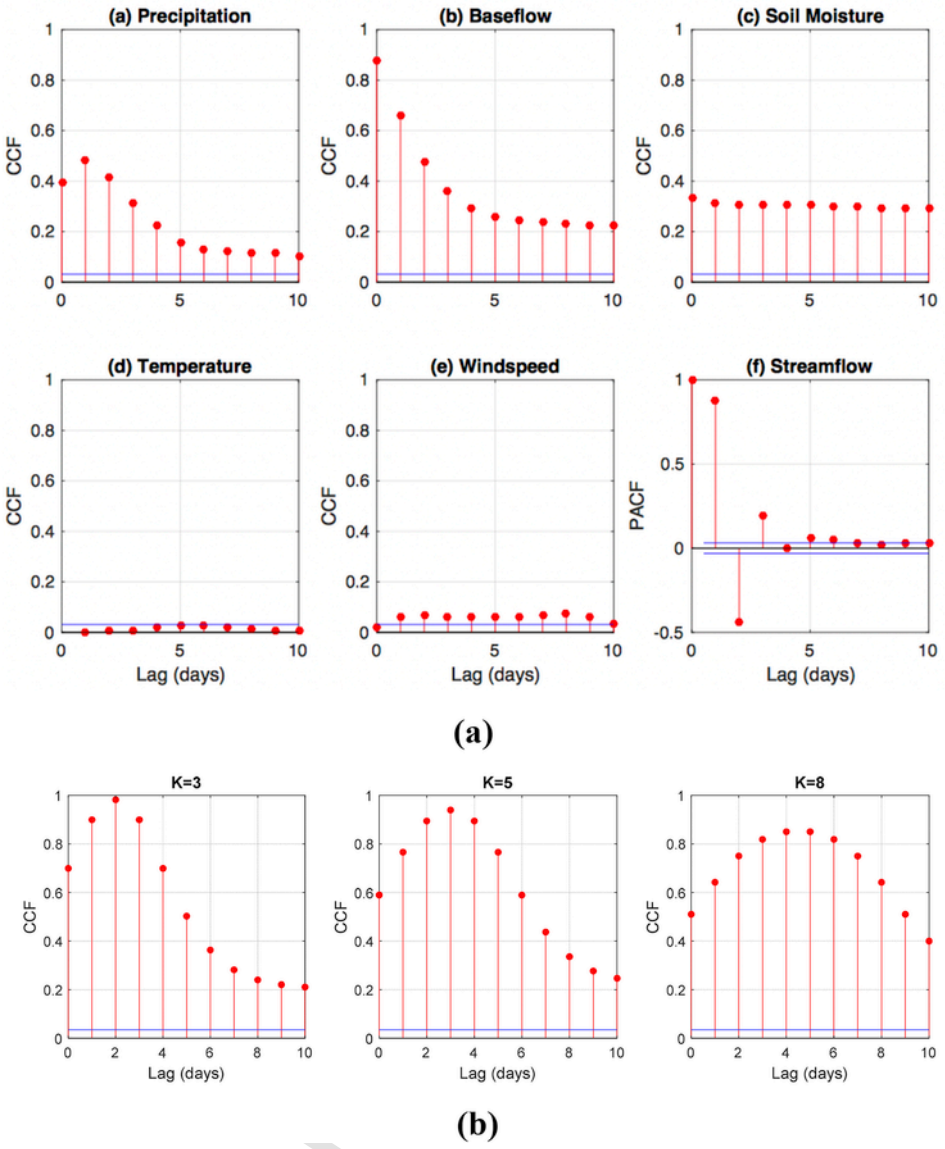

Fig. 4. Upper panel (a) Cross-correlation functions (CCF) between with observed reservoir streamflow and antecedent (a) precipitation, (b) baseflow, (c) soil moisture, (d) temperature, (e) wind speed, and (f) Partial autocorrelation function for streamflow. **Lower panel (b)** CCF for antecedent moving average inflow over different window lengths against observed flow for Pensacola dam over the training period. The blue lines show 95% confidence bands around zero. (For interpretation of the references to colour in this figure legend, the reader is referred to the Web version of this article.)

based on the window size. For each lead-time, the window size giving the best cross-correlation was identified to obtain the optimal K value.

Based on this CCF based analysis, following values were selected for antecedent moving averaged streamflow: $K = 3$ for lead times of 1 and 2 days, $K = 5$ for lead time of 3 days and $K = 8$ for lead times of 4–7 days. Three days of antecedent streamflow were also used for forecasting beyond lead-time of 3 days. Two and three days of antecedent precipitation and baseflow were considered, respectively, while the temperature, soil moisture and windspeed were ignored due to lower CCF values. In applying the filter for baseflow separation, the values of 0.05 and 0.73 were found for a and BFI_{max}, respectively using a trial-and-error procedure for Pensacola dam. In addition to these antecedent variables, the forecast forcings of precipitation and temperature (minimum and maximum) were also provided as input nodes to ANN pertaining to the respective lead time of forecasting.

Next, to select the final set of input nodes and to assess the relative contribution of each predictor, the ANN was simulated with different combinations of predictors. This demonstrates the structural validity of the selected model as explained in section 3.4. The configuration was kept same across all the dams to allow fair assessment across all 23 dams and keep the sensitivity analysis simple. The sensitivity analysis is also advantageous as it can inform if the ANN model trained using a particular set of inputs is robust enough to be scalable to locations with varying characteristics.

For assessing the performance, the NSE was calculated for each lead-time of the modeled flow. Using the ANN configuration that yielded the highest average NSE across all the dams, the best combination of input nodes was derived. The period of Jan 2007 to Aug 2014 was used as the *training set*, while the *validation* and *testing sets* extended from Sep 2014–Oct 2015 and Nov 2015–Dec 2017, respectively. Table 2 demonstrates the sensitivity analysis carried out with the different configurations, tabulating the average NSE values for lead times of 1, 4 and 7 days over all the dams during the testing period. The individual dam NSE values are shown only for Pensacola and Green Peter dams for the sake of brevity, for the lead times of 1 and 7 days.

Table 2 gives the value that each individual predictor adds to the ANN forecast skill. It can be seen that, although the antecedent and forecast precipitation and temperature have little value by themselves,

Table 2
NSE (testing period) averaged for all 23 dams and examples for two dams, using different predictor combinations. P_a: antecedent precipitation (2 days), P_f: forecast precipitation (1 day), T_f: forecast min and max temperature (1 day each), B: antecedent baseflow (3 days), Q: antecedent streamflow (observed/moving-averaged). The row in bold is the selected best combination.

Predictor Combination	Average NSE (all 23 dams)			Pensacola Dam		Green Peter Dam	
	L1	L4	L7	L1	L7	L1	L7
P_a,T_f	0.095	−0.030	−0.036	0.269	0.132	0.437	0.173
P_f,P_a,T_f	0.177	0.108	0.063	0.370	0.128	0.529	0.324
B	0.670	0.371	0.286	0.470	0.175	0.751	0.280
Q	0.652	0.347	0.272	0.683	0.183	0.752	0.292
Q,B	0.669	0.366	0.253	0.812	0.151	0.757	0.319
T_f,Q,B	0.551	0.416	0.327	0.598	0.256	0.766	0.411
P_f, P_a, T_f, B	0.730	0.451	0.231	0.815	0.252	0.897	0.482
P_f,P_a,Q,B	0.771	0.396	0.306	0.799	0.164	0.889	0.459
P_a,T_f,Q,B	0.654	0.331	0.327	0.762	0.202	0.746	0.460
P_f, P_a, T_f, Q, B	**0.743**	**0.481**	**0.342**	**0.838**	**0.268**	**0.910**	**0.455**

they generally improve the performance when used in combination with the flow variables. Although exceptions exist to this trend when only NSE is considered as a measure of performance as in Table 2, the skill is improved in terms of minimized lag between the peaks in the modeled and observed flow. This is more visible from the lagged correlations between the two streamflow time series plotted in Fig. 5, where higher correlation value close to lag 0 represents better performance with reduced peak time lagging. Using only the base flow and moving average flow as predictors (Fig. 5(a and b)), the peak correlation occurs at a higher lag due to which the modeled peaks exhibit time lagging. However, as Fig. 5(b, d) show, the lag is reduced significantly when forecast precipitation and temperature are included. The correlation values at lag 0 increase in the latter combination.

Based on this analysis, the final predictor combination for the ANN is selected as: antecedent precipitation (2 days), antecedent baseflow (3 days), antecedent streamflow (3 days; for lead times of 4–7 days), antecedent moving average flow (3-, 5- and 8-day window based on lead time), forecast precipitation (1 day) and forecast min/max temperature (1 day each). The final ANN architecture selected is shown in Fig. 6.

4.2. ANN-based forecast assessment

Using the optimal combination of predictor nodes from section 4.1, the ANN model was simulated for the selected 23 dams and the skill in forecast was assessed using various metrics of evaluation over the testing period.

To assess the predictive validity, the evaluation of the modeled flow was performed over completely independent test set using metrics of NSE, Correlation, and MAE. Table 3(a) summarizes the metrics for each of the 23 dams. The six stations on Ganges, Brahmaputra and Mekong river basins over which the ANN model was setup are also included in the evaluation for the sake of comparison in Table 3(b). The plots of the observed and modeled flow time series are shown in Fig. 7.

The replicative validity is assessed using (i) scatter plot of observed and modeled flow, and (ii) time series of standardized residuals. Scatter plot of the observed and modeled flow data in Fig. 8(a) shows robust performance, where systematic divergence from the 1:1 line indicates unmodeled behavior. The time series of the standardized residuals, as

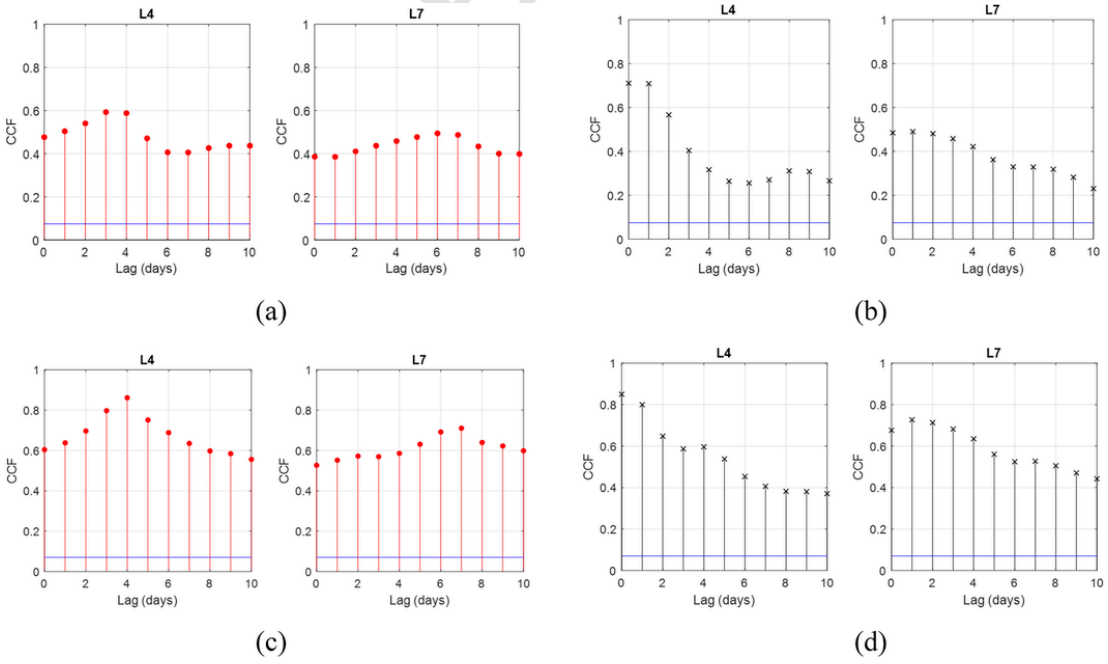

Fig. 5. Lagged cross-correlations between the modeled and observed streamflow for Pensacola dam using **(a)** only base flow and moving average flow, **(b)** using also the antecedent/forecast precipitation and temperature as predictors in addition to antecedent flow. **(c)** & **(d)** same evaluation but for Green Peter dam. Higher correlation value close to lag 0 represents better performance with reduced peak time lagging. Blue lines mark 95% confidence bands around zero. (For interpretation of the references to colour in this figure legend, the reader is referred to the Web version of this article.)

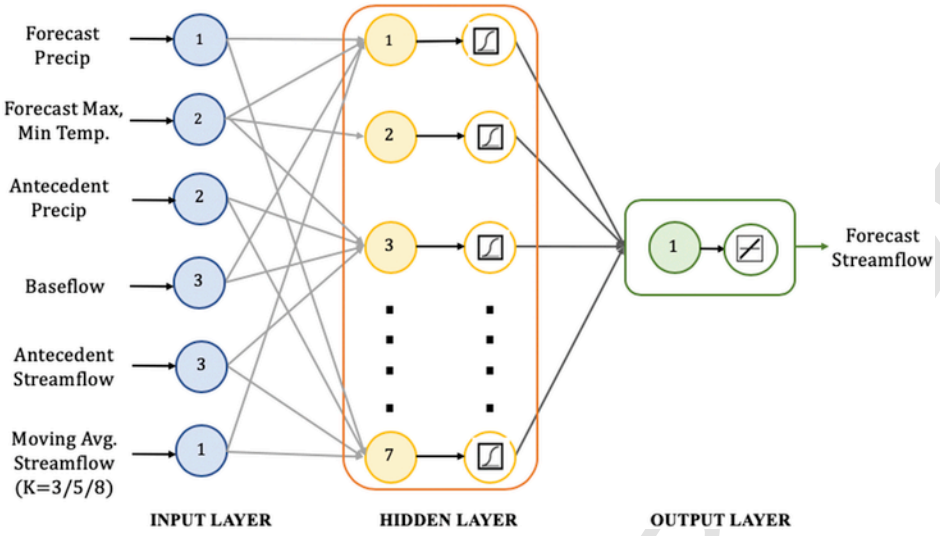

Fig. 6. Three-layered ANN architecture and the selected input nodes with log sigmoid and linear transfer functions for hidden and output layers, respectively. Numbers on input nodes represent selected number of antecedent/forecast days. *K* is the window length for moving average streamflow that is varied with lead time of forecasting.

Table 3a
Evaluation of ANN flow forecasts for 23 dams stating NSE, Correlation and MAE for lead times of 1, 4 and 7 days.

	Dam Name	NSE			Correlation			MAE (cfs)		
		L1	L4	L7	L1	L4	L7	L1	L4	L7
1	Libby	0.974	0.871	0.780	0.987	0.933	0.886	1256.2	2413.7	3325.6
2	Jackson	0.958	0.850	0.771	0.979	0.922	0.880	223.2	411.9	519.7
3	Dworshak	0.955	0.812	0.681	0.978	0.902	0.828	707.8	1698.2	2370.5
4	Hungry Horse	0.920	0.746	0.649	0.960	0.873	0.822	665.1	1199.4	1462.6
5	Navajo	0.917	0.819	0.703	0.960	0.905	0.841	221.2	345.7	468.0
6	Great Salt	0.910	0.754	0.455	0.956	0.872	0.684	278.9	541.8	821.2
7	Lost Creek	0.908	0.711	0.580	0.953	0.852	0.767	179.2	382.8	466.0
8	Cougar	0.885	0.496	0.456	0.942	0.735	0.682	129.4	302.0	354.6
9	Hills Creek	0.864	0.670	0.502	0.930	0.827	0.714	193.2	376.6	444.3
10	Detroit	0.843	0.720	0.606	0.920	0.849	0.780	364.5	553.0	703.0
11	Pensacola	0.838	0.517	0.268	0.922	0.724	0.519	3031.8	5545.8	6697.6
12	Fort Peck	0.777	0.329	0.240	0.883	0.584	0.539	792.6	1542.3	1955.3
13	Mud Mountain	0.746	0.280	0.406	0.868	0.534	0.639	329.3	606.7	501.4
14	Howard	0.717	0.457	0.238	0.859	0.819	0.550	318.7	419.8	505.6
15	Buford	0.678	0.465	0.326	0.835	0.704	0.578	584.3	863.0	791.2
16	Hartwell	0.632	0.433	0.340	0.799	0.693	0.604	1456.6	1951.5	2072.3
17	Carters	0.624	0.414	0.242	0.835	0.689	0.521	218.6	277.6	310.8
18	Allatoona	0.571	0.524	0.376	0.769	0.726	0.617	705.8	597.1	749.5
19	Eldorado	0.566	0.100	0.036	0.769	0.326	0.223	176.2	257.7	287.7
20	Green Peter	0.531	0.331	0.133	0.741	0.611	0.427	219.6	295.7	336.4
21	Broken Bow	0.517	0.167	0.140	0.731	0.408	0.388	820.9	1355.2	1484.6
22	Fort Supply	0.246	−0.33	−0.29	0.68	0.389	0.267	11.8	16.3	15.1
23	Marion	0.323	−0.092	0.063	0.630	0.365	0.254	89.0	129.1	115.1

plotted in Fig. 8(b) identifies any serial correlation in the residuals that suggests unmodeled deterministic behavior. The standardized residuals were calculated as raw residuals divided by their estimated standard deviation. An ideal plot of residuals should lie randomly within a horizontal band with no visible patterns.

Figs. 7 and 8 suggest that the forecast skill decreases with increasing lead-time as expected, however the scatter plot of the observed and modeled flow fits well across the 1:1 line. The standardized residuals are mostly randomly distributed around the zero line, though the peak flow season has a few negative residual points for lead times of 4 and 7 days, corresponding to the underestimations in modeled flow. The performance for Pensacola dam is specifically affected by an unusually extreme peak event that hit the reservoir during the testing period, the likes of which did not occur over the training set of data. This causes heavy underestimations in the flow forecast over the event. A longer training period is required to improve the performance over such extreme peak flow events. Apart from this exceptional peak event, serial correlation in the residuals is mostly minimal across dams.

After assessing model validity, the next step in the ANN performance assessment is to compare the performance across the 23 dams (and 6 large-scale basin stations) as a function of dam's hydrologic and climate characteristics. Three factors were used to capture the varying characteristics –upstream drainage area of dam, local climate according to Köppen-Geiger climate classes, and coefficient of variation (COV) of observed streamflow, defined as ratio of the standard deviation of the inflow time series (over training period) to its mean value. COV is a measure of variability of the incoming flow into the reservoir. Fig. 9(a) below plots the distribution of NSE values for lead-time of 1 and 7 days (measure of ANN performance) over the testing period, as a function of the COV for each dam. The respective climate class-based distribution of the NSE values for each dam is shown in Fig. 9(b). COV is shown on the same plot in the bottom panel.

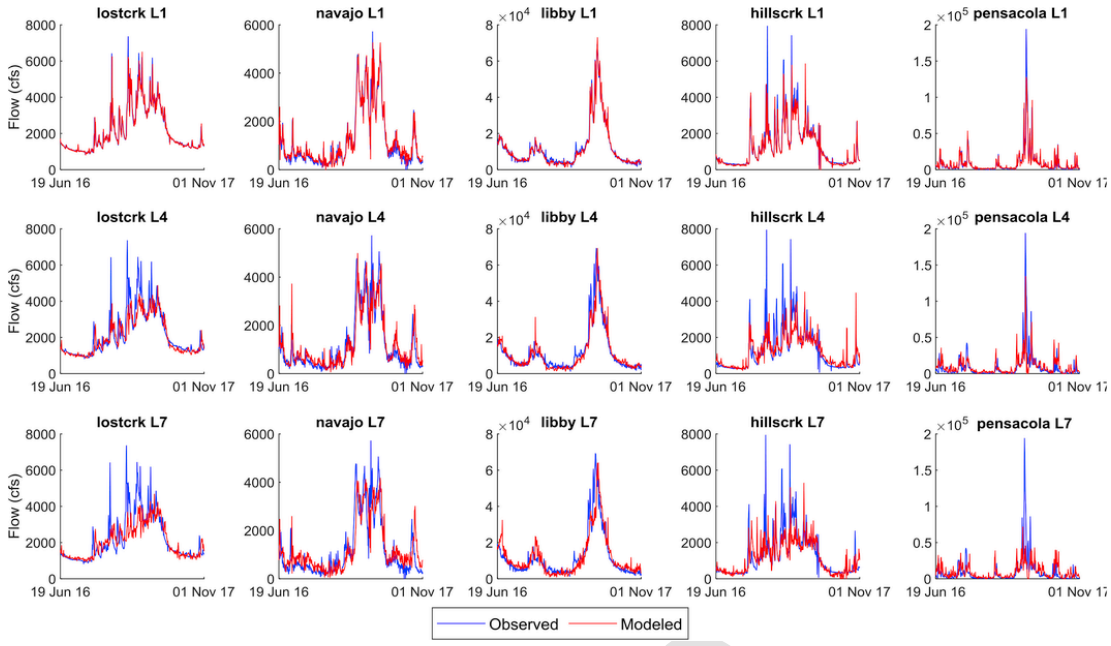

Fig. 7. ANN modeled flow plotted against observed values over testing period for 1, 4, and 7-days lead time (L1, L4, and L7) for Lost Creek, Navajo, Libby, Hills Creek and Pensacola dams.

Fig. 9(a) reveals strong negative signal between the COV and forecast skill. The six stations in large river basins perform very well (Table 3(b)) with much larger catchment areas and smaller variation in flow due to monsoonal hydrology. From Fig. 9(b), it is evident that the performance improves as the drainage area increases especially for the cold humid and humid subtropical class dams. The Mediterranean class dams perform well even for smaller reservoirs due to the similar flow characteristics in all the four dams (COV ~1 and mean flow ~1500cfs). Appendix A shows the map of climate class with ANN performance for each dam. The two exceptions from the expected trend, encircled in red, are explained below:

1. The Fort Supply dam, in humid subtropical climate, receives very low flows with a mean value of 43 cfs over the training period and 18 cfs over validation/testing, leading to high COV. This results in offsetting the effect of average drainage area and makes it harder for ANN to learn the flow pattern.
2. The Fort Peck with drainage area is 149,508 km^2 (not shown entirely in Fig. 9(b) due to scaling issues) is the only dam to have a few regulating flow structures upstream. A part of annual inflow is contributed by the releases from other upstream dams in addition to the natural unregulated component, which deteriorates the NSE value at higher lead times and again counterbalances the effect of very high drainage area.

4.3. ANN-based ensemble forecasts

Feeding the ANN with ensemble of forecast predictors from GEFS resulted in ensemble members of the forecast flow and estimates of flow uncertainty. The spread and mean of the forecast flow were calculated. The application is demonstrated over a single peak flow event for three dams. These are: (i) Pensacola dam with peak event of May 2015, (ii) Detroit dam with peak event of Dec 15, (iii) Jackson dam with peak event of May-Jun 2016. The results of ensemble forecasts compared with the deterministic (using GFS forcing fields from section 4.2) and observed flows are shown in Fig. 10. The mean of the ensemble forecasts usually corresponds well with the deterministic forecasts except during the high flow events when the ensemble spread is higher. The increase in forecast flow uncertainty with lead-time is also visible from Fig. 10 for the selected dams.

4.4. Reservoir operations optimization using deterministic forecasts

To demonstrate the optimization of reservoir operations based on the ANN-based forecasts, the Pensacola dam was selected. A schematic of dam specifics with key operating constraints is shown in Fig. 11(a). The observed data of inflow, releases and hydropower generation were obtained from the USACE (Monthly Charts for Grand Lake, 2018).

4.4.1. Forecasts based Model Predictive Control scheme

The optimization using data-driven inflow forecast was performed over a period of two years (Sept 2014–Aug 2016) for Pensacola Dam. The period was selected to ensure it does not entail the training set of ANN. The optimization problem is solved at each time step applying NSGA-II technique, yielding the optimal release sequence for the horizon of 1–7 days. With the MPC strategy, the first of these is implemented in simulation and the remainder are subsequently updated next day when a new forecast is issued. A balanced optimum solution was chosen on the Pareto front for flood and non-flood seasons to maximize hydropower and minimize the penalty function. An example Pareto-optimal solution front between the hydropower deficit minimization and penalty function (in terms of deviation from rule curve) and a sample balanced solution over the front is shown in Fig. 11(b). The optimized release decisions over the 2-year period are compared with the actual observed operations in Fig. 12(a), while the resulting reservoir headwater levels based on optimized and observed releases are compared in Fig. 12(b).

4.4.2. Benchmark scheme

The benchmark operating scheme, in the form of control rules or look-up table, was designed to assess the performance of optimized operations based on forecasts. The computations over the 24-year period (1995–2018) at monthly time step were performed using the R package '*reservoir*' (Turner and Galelli, 2016) with the '*sdp_hydro*' function that implements Stochastic Dynamic Programing under given constraints and constants. Release was discretized into 50 uniform values up to the maximum release threshold (see Appendix B), while the storage was

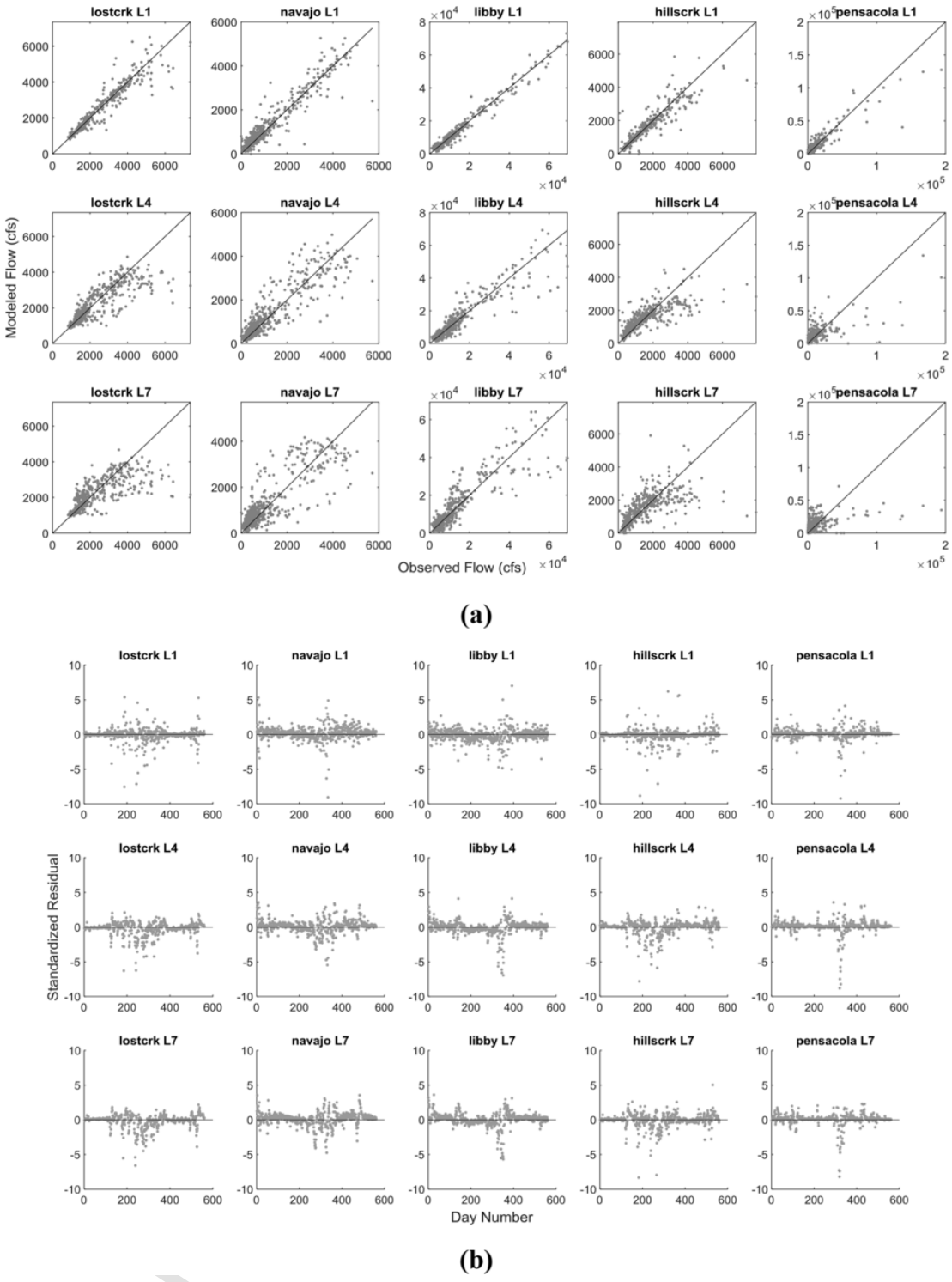

Fig. 8. **(a)** Scatter plot of the forecast and observed flow for 1, 4 and 7-days lead times; **(b)** Standardized residuals plotted with time over testing period to identify serial residual correlation for Lost Creek, Navajo, Libby, Hills Creek and Pensacola dams.

discretized into 200 values within the set bounds. Fig. 13 shows the optimal release decisions, storage behavior and power generated under control rules.

4.4.3. Comparison of forecast-based optimization with the benchmark

To assess the optimization performance, two hydropower benefits were calculated: (i) *optimized HP*: hydropower generation resulting from the optimized releases based on the ANN inflow forecasts while passing the observed inflow into the system; (ii) *benchmark HP*: hydropower generated from benchmark control rules-based operations. Over the two years of assessment (Sep 2014–Aug 2016) that includes flood and non-flood seasons, the *optimized HP* was 954,061 MWh in comparison to the *benchmark HP* of 906,807 MWh. Thus, the optimized release decisions resulted in an additional and 'flood-safe' hydropower production of 47,253 MWh amounting to $4,611,892 using the average residential electricity rate in Oklahoma City of 9.76¢/kWh (Electricity

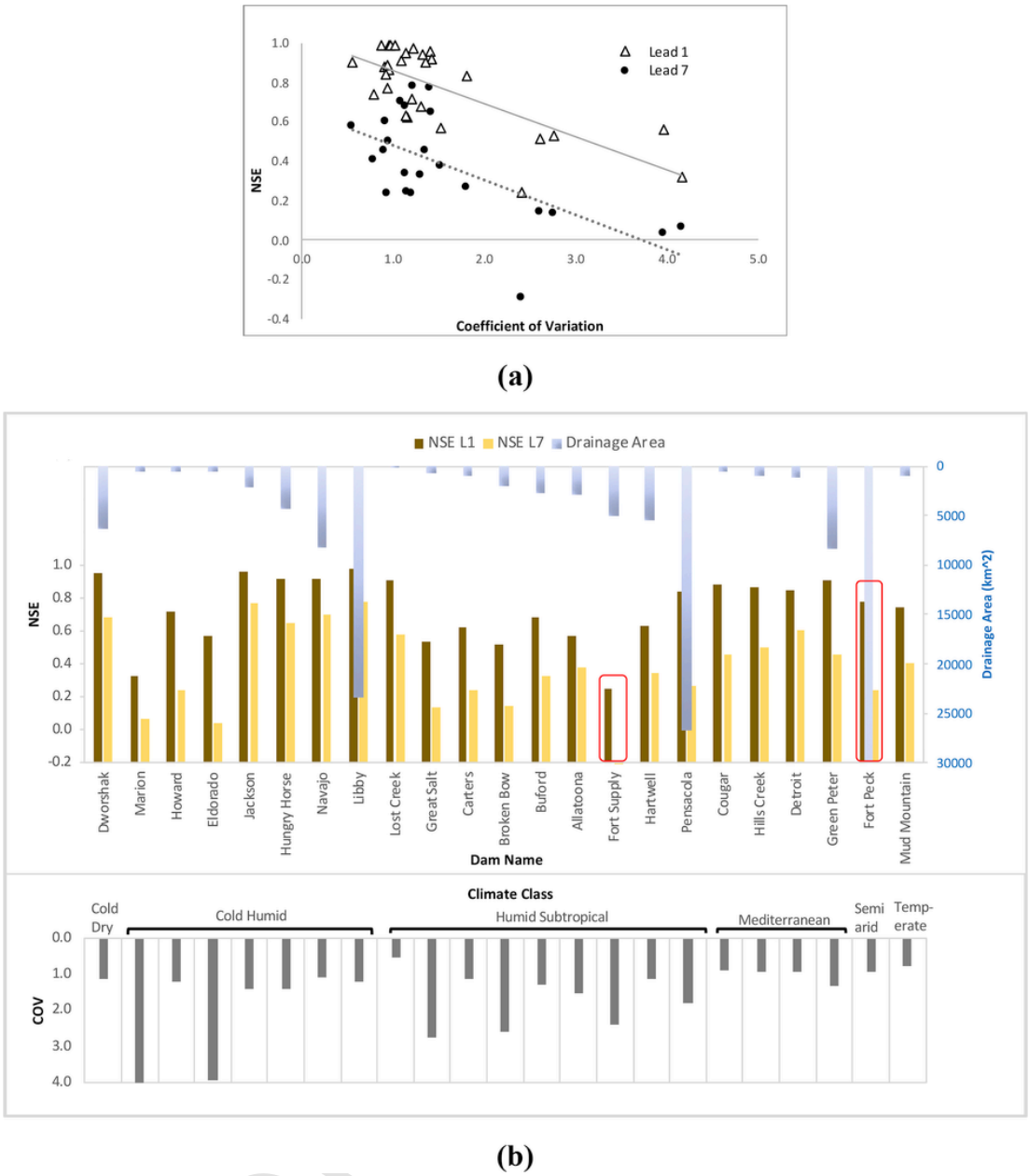

Fig. 9. **(a)** ANN performance in terms of NSE values at lead time of 1 and 7 days (L1 and L7) plotted against the coefficient of variation (COV) for all the 23 dam sites including the additional 6 large-scale basin stations. **(b)** Distribution of NSE values (left y-axis) for each dam at L1 and L7 with drainage area (right y-axis) in the upper panel. The respective local climate class and COV is plotted in the lower panel. The dams in each climate class are sorted in order of decreasing drainage area. The two exceptions – Fort Supply and Fort Peck not following the expected trend are encircled in red. (For interpretation of the references to colour in this figure legend, the reader is referred to the Web version of this article.)

Table 3B
Evaluation of ANN flow forecasts for six stations of Ganges, Brahmaputra and Mekong river basins, comparing the NSE and Correlation.

#	Station Name	NSE			Correlation		
		L1	L4	L7	L1	L4	L7
1	Hardinge Bridge	0.945	0.936	0.930	0.973	0.969	0.965
2	Bahadurabad	0.892	0.893	0.872	0.945	0.945	0.934
3	Vientiane	0.990	0.880	0.810	0.990	0.940	0.910
4	Pakse	0.990	0.950	0.890	1.000	0.980	0.950
5	Stung Treng	0.990	0.940	0.900	1.000	0.970	0.950
6	Kampong Cham	0.990	0.960	0.900	1.000	0.980	0.960

Rates, 2018). At an average electricity consumption of 900 kWh per month per US household, this much of energy can fulfill the demands of around 45,530 households for one month.

For the penalty function addressing flood control during peak flow seasons, two peak events in the two-year period of assessment were analyzed for the improvement in peak release reduction. The ANN forecast flow over each of these events is shown in Fig. 14.

The underestimation is much higher in the second peak flow event with increasing lead-time as the event of such a magnitude is quite rare making it difficult for ANN to learn. Due to this underestimation, as the optimization over 7-day horizon proceeds, the pre-event releases are triggered only very close to the event and not much improvement is achieved in downstream flood control. While on the contrary, for the May 2015, with better forecast skill, the optimal releases are bounded within the safe threshold of 30,000 cfs for most days and the peak re-

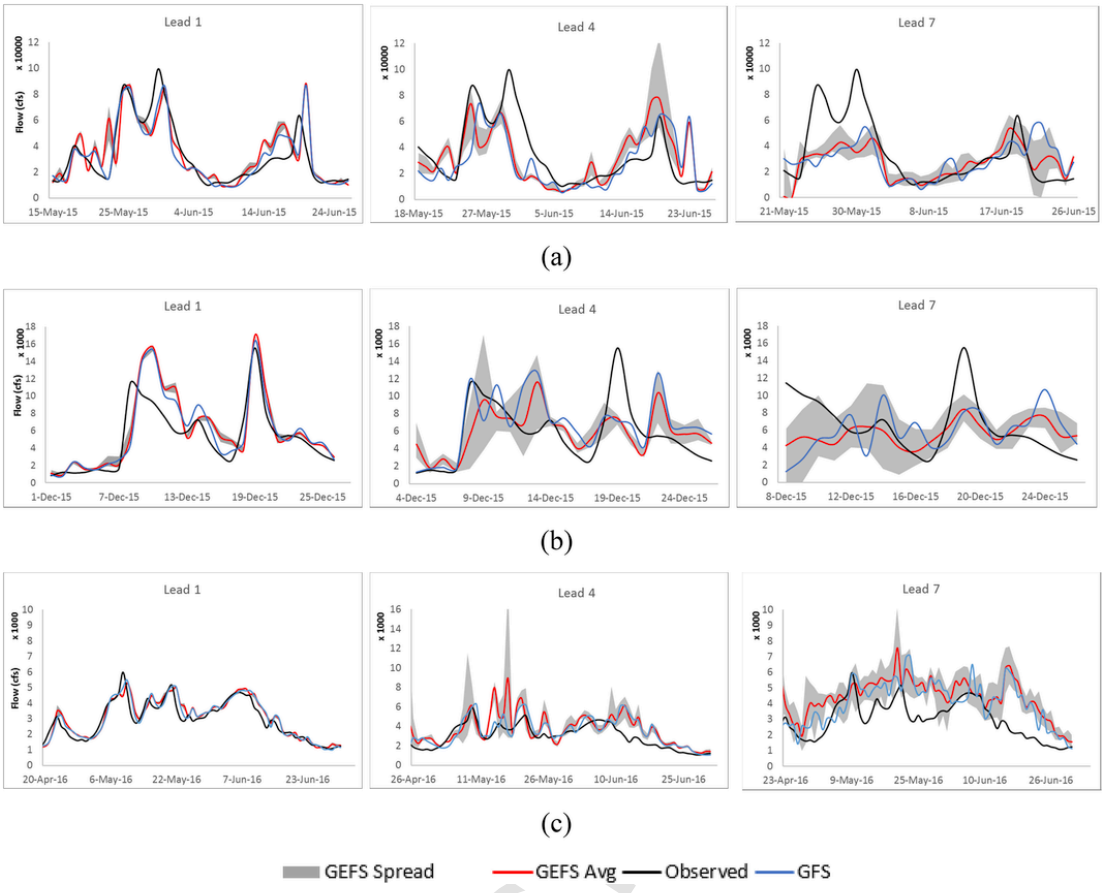

Fig. 10. Ensemble forecasts (average and spread) obtained by feeding ANN with ensemble forecast fields from GEFS, compared with the observed flow and deterministic forecasts (feeding ANN with GFS forecasts) for: **(a)** Pensacola dam, **(b)** Detroit dam, and **(c)** Jackson dam, at lead times of 1, 4 and 7 days.

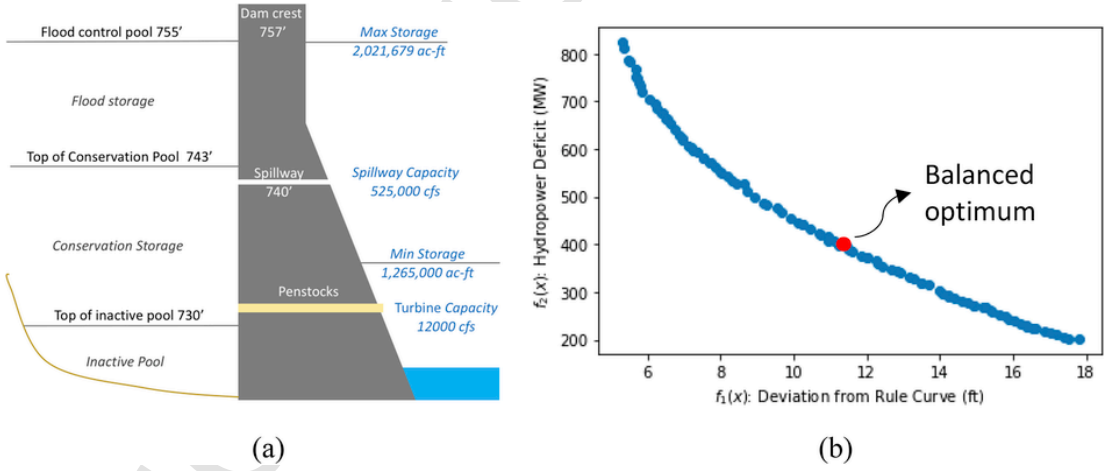

Fig. 11. **(a)** Specific pools and constraints used for optimization with pool levels above mean sea level; **(b)** Solutions on the Pareto front and a sample balanced optimum between the energy maximization and penalty function for Pensacola Dam in Oklahoma.

lease reduced by ~18%–80,000 cfs on May 30 (see Fig. 12(a)). The operations improved in terms of the resulting reservoir levels being closer to rule curve as compared to the observed operations during drawdown and dry seasons, as shown in Fig. 12(b).

4.5. Reservoir operations optimization using ensemble forecasts

The ensemble of the forecasts was assimilated into the reservoir operations optimization. The optimization model as setup in section 4.2 was simulated with three scenarios of GEFS-based forecast flow – the minimum, maximum and average of the ensemble inflow members. The technique is illustrated using the peak flow event of May 2015 over Pensacola dam. The GEFS ensemble-based inflow forecasts, as shown earlier in Fig. 10(a), were used to simulate the optimization model. The optimized releases and resulting reservoir elevations from each ensemble scenario and from previously obtained GFS-based forecasts are plotted in Fig. 15.

Figs. 15(a) and Fig. 10(a) suggest that the uncertainty in inflow forecasts, which is minimal for lead-time of 1 day and increases afterwards, translates into the corresponding uncertainty in the release deci-

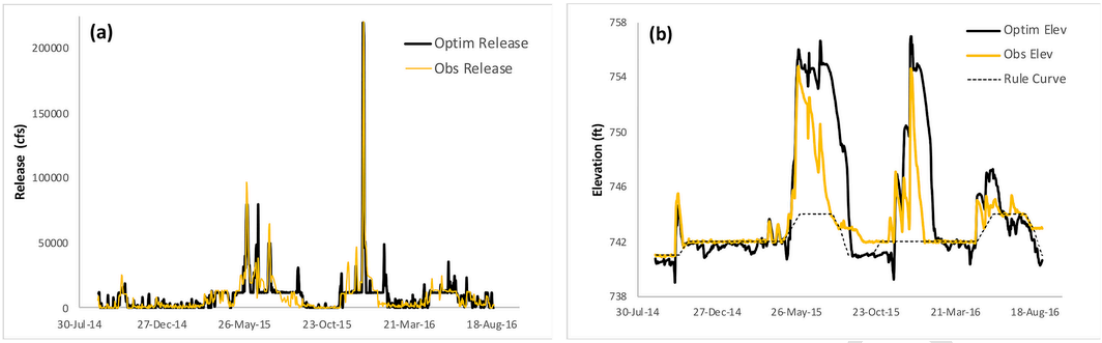

Fig. 12. **(a)** Optimized release policy using the ANN forecasted inflow, compared with the observed operations; **(b)** Resulting reservoir headwater levels using optimized and observed releases, and the rule curve for Pensacola dam from USACE.

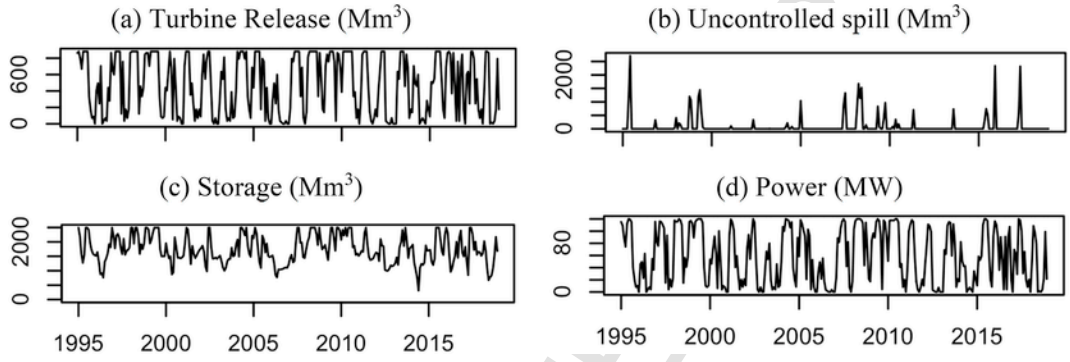

Fig. 13. Reservoir operating policy and resulting reservoir behavior at monthly scale based on the benchmark control rules designed specifically for hydropower maximization neglecting the forecasts using the R package '*reservoir*' (after Turner and Galelli, 2016).

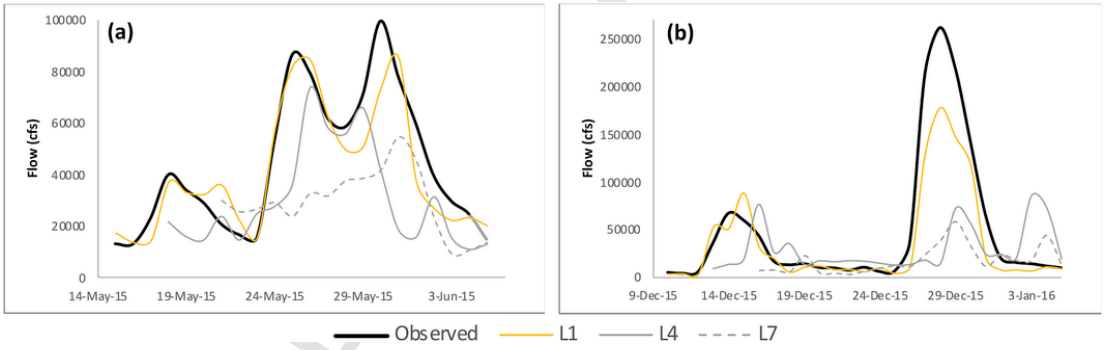

Fig. 14. ANN forecast flow for lead times of 1, 4 and 7 days over the Pensacola dam's peak inflow events of **(a)** May 2015 with peak flow of 99,700 cfs and **(b)** Dec 2015 of 221,360 cfs.

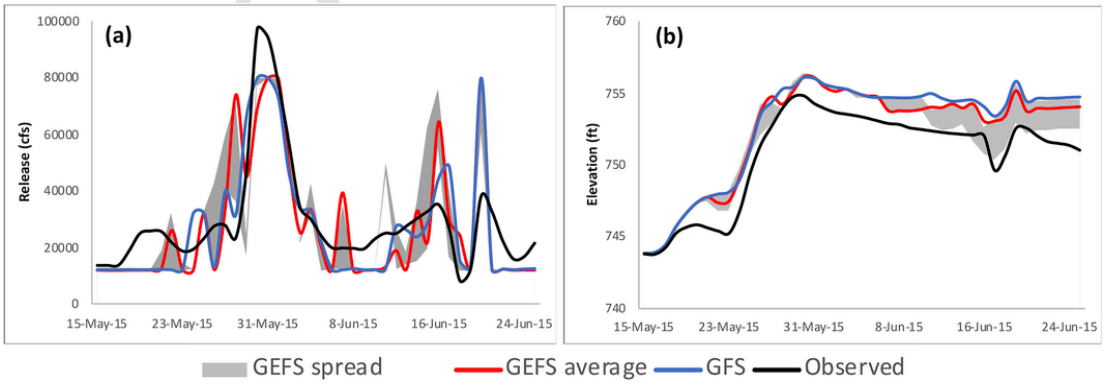

Fig. 15. Optimized release decisions using rolling horizon optimization and resulting reservoir elevation behavior based on average, min and max of the GEFS ensemble flow forecasts. Spread is obtained based on the minimum and maximum values of the optimized variables. The respective variables from GFS based deterministic forecasts and observations are also shown.

sions. However, as the optimization proceeds on a rolling horizon basis, the more certain and skillful forecasts are ingested to generate optimal release decisions that minimize the uncertainty in the policy and resulting reservoir storage behavior.

5. Discussion and conclusions

A data-driven weather forecast-based reservoir inflow forecasting using ANN technique was developed with a comprehensive validation and testing framework. The scalability of the concept was proven by applying it over an inventory of 23 dams receiving unregulated natural inflow with varying hydrological and climate characteristics. A consistent ANN architecture and input predictor configuration was used to allow a fair comparison across dams. In addition to the antecedent conditions, short-term forecast fields from the GFS model were used as inputs to train a three-layered ANN. Using a transformation of antecedent flow time series along with the forecast fields improved the peak flow estimation with minimum time lagging. Six stations (with no dams) on large river basins of Ganges, Brahmaputra and Mekong were also included in the assessment. Superior performance was observed for these international basins due to their large basin area and strong seasonal hydrology due to the predictable monsoon. The forecast skill assessment suggested that the technique performs reasonably well with NSE value greater than 0.5 for 48% of the sites (including those on larger basins) for forecasts at lead-time of 7 days. This suggests that the same ANN configuration is able to capture the flow variations across a variety of dams.

The performance across the different dams also revealed trends pertaining to flow characteristics and area of the upstream catchment. As reservoir receives inflow that is more variable over the annual scale with less visible seasonal patterns, reflected by a high COV value, the forecast performance decreases. This can be explained as the ability of ANN to learn from the limited training provided in this study is not sufficient when the variability in the flow is too high. An improved performance can be achieved for such basins using a longer training period with varying flow regimes. Apart from COV, another factor controlling the flow characteristics and the forecast skill is the drainage area of the basin. Decreasing drainage area makes the basin hydrologically more responsive with lower times of concentration and the basin generates flashier peak flows with lesser seasonal patterns. This deteriorates the forecast skill especially with the increasing lead-times. Furthermore, although the performance of dams in Mediterranean climate zone is generally better than dams in other climates, there is no remarkable trend as a function of local climate. This in fact verifies the robustness of the selected ANN architecture's learning ability across diverse hydro-climatologic conditions. The results also prove the global scalability of the proposed technique, as the forecast performance was tested here for a wide range of hydrologically different dam sites (as well as undammed river stations in large river basins of Asia) and in different climates. A comparison of the proposed ANN approach against simpler modeling techniques (such as a linear regression or conceptual rainfall-runoff model) will further underscore its value and will be a focus of future study.

As the deterministic flow forecasts from ANN model were not able to capture the inherent uncertainty present in the streamflow estimates, an ensemble of forecast fields was assimilated into the trained ANN to propagate the uncertainty. The results revealed that the highest spread in ensemble flow forecasts occurs during the peak flow seasons when the inflow into reservoir is most uncertain. This is the regime when the dam operators can benefit most from these forecasts. Providing the operating agencies with the ensemble forecasts during flood seasons can help increase the odds of operating for the flows of high probability of occurrence and improve the energy generation without risking the flood control.

The forecasting technique was then coupled with a reservoir optimization model for maximizing the hydropower generation without compromising flood control and dam safety. A rolling horizon scheme was employed to obtain optimal release policy over the horizon of 1–7 days. A benchmark policy, obtained as look-up table by neglecting the forecasts but optimized for energy generation, provided a fair benchmark to compare hydropower benefits from the forecast-based optimal operations. The long-term assessment over two years yielded significant benefit over the benchmark policy with reduced flood risk downstream.

Short-term ensemble forecasts were also explored in this study. The reservoir operations optimization model was also simulated using the different scenarios (min, max and average) of the flows over the forecast horizon. The uncertainty in the release decisions was propagated by the corresponding spread of the ensemble forecast flows, although the effect was undermined due to the continual updating of forecasts every day during the optimization process. It should be mentioned that uncertainty (spread) in the ensemble flow forecasts, which is highest at times of extreme peak flow, also leads to the uncertain operating policy mostly during the peak flow times. This implies that the use of ensemble forecasts can be most efficient during the seasons of high flow and should be avoided over drier periods.

The proposed ANN scheme that is numerically fast and efficient for forecasting of reservoir inflow allowed an assessment over multiple years and multiple sites using computationally modest resources. The proposed ANN technique is appropriate for global scale operationalization of short-term reservoir inflow forecasts for any dam site provided the training data are selected carefully with acute hydro-climatic understanding of the basin. The inputs used herein are freely and globally available. Such a technique also allows long-term risk assessment of historical operations by directly incorporating the forecast fields from NWP models. The optimization using Pareto optimality concept allows the operator to choose an appropriate optimal solution depending on the prevailing circumstances and analyzing the tradeoff between the conflicting objectives. Future work will constitute exploring this concept for network of dams that are operated as a system (such as the Colorado or the Columbia River system). Another future extension of this work is to connect energy demand forecasting and energy market pricing with the ANN-based reservoir operations optimization. A key component towards operationalization is dissemination of the outcome into a form useful for the operating agencies and practitioners so that the results and advisory become locally actionable. Our future research plans to address these issues and report them in a future study.

Appendix A. ANN Performance with Köppen Geiger Climate Classes

The climate classes used in this study are shown in the map below, with the distribution of selected dam sites. The markers for each site are sized with the NSE of ANN forecast at lead time of 1 day.

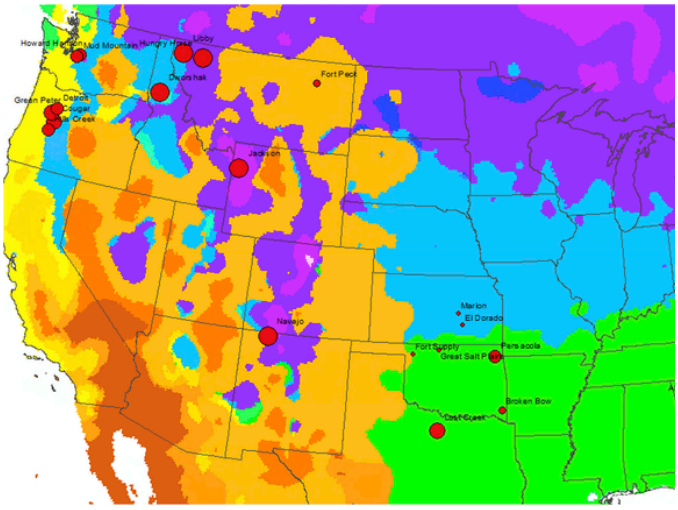

Fig. A1. Map showing the Köppen Geiger Climate Classes used in this study and the selected dam sites with markers sized with NSE of ANN forecasted flow at lead time of 1 day.

Appendix B. Optimization model setup for Pensacola Dam

Constraints – Mathematical Formulation

We define the following constraints for the optimization model with the specific values summarized in Table B1.

1. Release from the turbines is constrained by the turbine capacity, P_{turb}.

$$R_{p,t} \le P_{turb} \ , \ \forall t \tag{B.1}$$

2. The system follows storage-volume continuity (water-balance equation) which requires that in each period t,

$$S_{t+1} = S_t + \left[I_t - L_t - \left(R_{p,t} + R_{np,t}\right)\right] \cdot \Delta t, \ \ \forall t \tag{B.2}$$

However, as the optimization is performed at daily time steps ($\Delta t = 1$), the losses due to evaporation and seepage, L_t, were ignored.

3. Reservoir storage was limited to ensure dam safety and avoid infeasible scenarios such as the reservoir running empty.

$$S_{min} \le S_t \le S_{max}, \ \ \forall t \tag{B.3}$$

Here, S_{min} is set up considering the conservation pool of the reservoir to keep it at a suitable level above the inactive pool, while S_{max} denotes the active storage capacity till the reservoir's full pool.

4. To prevent the downstream flooding hazards, the total release was constrained to a maximum limit, R_{max},

$$R_{p,\,t} + R_{np,t} \le R_{max}, \ \forall t \tag{B.4}$$

5. To avoid excessive and infeasible rates of non-power release via the spillway, the non-power release rate was limited to the spillway capacity,

$$R_{np,t} \le Spill_{max}, \quad \forall t \tag{B.5}$$

6. Lastly, the releases made from reservoir should comply with the environmental flow limit, Q_{env},

$$R_{np,\,t} + R_{p,t} \ge Q_{env}, \ \forall t \tag{B.6}$$

Table B.1
Constraints for Optimization for Pensacola dam, OK

Constraint	Value	Comments
Turbine Capacity	12,000 cfs	–
Spillway Capacity	525,000 cfs	–
Minimum storage	1,265,000 ac-ft	95% of 10-yr minimum
Maximum storage	2,021,679 ac-ft	Flood control pool
Maximum release	50,000 cfs if level exceeds 750 ft, otherwise 30,000 cfs	Avoid flooding at downstream station of Neosho River
Env. flow limit	500 cfs	–

Objective Functions – Mathematical formulation

The following two functions (objective and penalty) were defined for setting up the optimization problem:

1. *Energy Maximization*: Minimize the deficit in hydroelectric energy production (MWh) from the maximum generation capacity of the powerplant,

$$\min f_1 = HP_{max} - \sum_t \varepsilon \cdot \left(HF_t - HT_t\right) \cdot R_{p,t} \cdot \Delta t_{turb} \tag{B.7}$$

2. *Penalty Function:* Minimize the sum of the absolute value of storage deviations from the rule curve-specified value over a fixed number of days of the optimization horizon. It is represented as,

$$\min f_2 = \sum_t \left|S_t - T_t\right| \qquad (t = 3, 4, \ldots 7days) \tag{B.8}$$

If a flood event is forecasted causing the reservoir level to reach the flood storage pool, the function is modified to minimize the uncontrolled spillway release,

$$\min f_2 = \sum_t R_{np,t} \qquad (t = 1, 2, 3, \ldots 7days) \tag{B.9}$$

where:

HP_{max} – Maximum hydropower generation capacity
HF – Reservoir forebay water level, obtained from area-elevation curve
HT – Reservoir tailrace water level
ε – Turbine efficiency
R_{np} – Spillway (non-power) release
R_p – Power (turbine) release
Δt_{turb} – Turbine operating hours

T – Target (rule curve specified) storage
S– Reservoir storage
t – Time step (days) over the period of optimization

Software availability

Name of the software ANN Reservoir Inflow Forecasting
Developer Shahryar Khalique Ahmad
Contact email skahmad@uw.edu
Contact Address Dept. of Civil and Environmental Engineering, Univ. of Washington, USA
Software required Matlab ® 2018b (needs Deep Learning Toolbox™, formerly Neural Network Toolbox™)
Available Since February 2019
Availability Matlab code and necessary dataset, available at:https://github.com/shahryaramd/ANN_FlowForecasting

Data availability

The type and source of the data set considered in this study.

Name of dataset	Data source (Developer)	Data format	Data availability
1. Pensacola dam inflow time series	US Army Corps of Engineers http://www.swt-wc.usace.army.mil/PENScharts.html	HTML webpage	Free
2. Forecast precipitation, temperature, windspeed	NOAA's Global Forecast System (GFS) model https://www.ncdc.noaa.gov/data-access/model-data/model-datasets/global-forcast-system-gfs	GRIB files	Free
3. Ensemble Forecast precipitation, temperature	NOAA's Global Forecast Ensemble System Reforecast (GEFS/R) model ftp://ftp.cdc.noaa.gov/Projects/Reforecast2	GRIB files	Free
4. In-situ precipitation, temperature	Global Surface Summary of the Day (GSOD) https://data.noaa.gov/dataset/dataset/global-surface-summary-of-the-day-gsod	Text files	Free
5. Gridded historical precipitation	Livneh daily CONUS data https://www.esrl.noaa.gov/psd/data/gridded/data.livneh.html	NetCDF files	Free

Appendix C. Supplementary data

Supplementary data to this article can be found online at https://doi.org/10.1016/j.envsoft.2019.06.008.

References

Ahmad, S.K., Hossain, F., 2018. Dynamic reservoir operations based on short-term weather forecasts for maximization of hydropower (Unpublished results). Journal of Renewable Energy

Akhtar, M.K., Corzo, G.A., Van Andel, S.J., Jonoski, A., 2009. River flow forecasting with artificial neural networks using satellite observed precipitation pre-processed with flow length and travel time information: case study of the Ganges river basin. Hydrol. Earth Syst. Sci. 13 (9), 1607–1618 https://doi.org/10.5194/hess-13-1607-2009.

Anctil, F., Perrin, C., Andréassian, V., 2004. Impact of the length of observed records on the performance of ANN and of conceptual parsimonious rainfall-runoff forecasting models. Environ. Model. Softw 19, 357–368 https://doi.org/10.1016/S1364-8152(03)00135-X.

Anghileri, D., Voisin, N., Castelletti, A., Pianosi, F., Nijssen, B., Lettenmaier, D.P., 2016. Value of long-term streamflow forecasts to reservoir operations for water supply in snow-dominated river catchments. Water Resour. Res. 52, 4209–4225 https://doi.org/10.1002/2015WR017864.

ASCE Task Committee on Application of Artificial Neural Networks in Hydrology, 2000. Artificial neural networks in hydrology. II: hydrologic applications. J. Hydrol. Eng. 5 (2), 124–137 https://doi.org/10.5121/ijsc.2012.3203.

Asif, M., Muneer, T., 2007. Energy supply, its demand and security issues for developed and emerging economies. Renew. Sustain. Energy Rev. 11, 1388–1413 https://doi.org/10.1016/J.RSER.2005.12.004.

Bartoletti, N., Casagli, F., Marsili-Libelli, S., Nardi, A., Palandri, L., 2018. Data-driven rainfall/runoff modelling based on a neuro-fuzzy inference system. Environ. Model. Softw 106, 35–47 https://doi.org/10.1016/j.envsoft.2017.11.026.

Birikundavyi, S., Labib, R., Trung, H.T., Rousselle, J., 2002. Performance of neural networks in daily streamflow forecasting. J. Hydrol. Eng. 7, 392–398 https://doi.org/10.1061/(ASCE)1084-0699(2002)7:5(392).

Bowden, G.J., Dandy, G.C., Maier, H.R., 2005. Input determination for neural network models in water resources applications: part 1 – background and methodology. J. Hydrol. 301, 75–92 https://doi.org/10.1016/j.jhydrol.2004.06.021.

Campolo, M., Andreussi, P., Soldati, A., 1999. River flood forecasting with a neural network model. Water Resour. Res. 35 (4), 1191–1197 https://doi.org/10.1029/1998WR900086.

Chen, D., Leon, A.S., Engle, S.P., Fuentes, C., Chen, Q., 2017. Offline training for improving online performance of a genetic algorithm based optimization model for hourly multi-reservoir operation. Environ. Model. Softw 96, 46–57 https://doi.org/10.1016/j.envsoft.2017.06.038.

Cheng, X., Noguchi, M., 1996. Rainfall-runoff modelling by neural network approach. Proc. Int. Conf. on Water Resour. & Environ. Res. 2, 143-15.

Cheng, C., Wang, S., Chau, K.-W., Wu, X., 2014. Parallel discrete differential dynamic programming for multireservoir operation. Environ. Model. Softw 57, 152–164 https://doi.org/10.1016/j.envsoft.2014.02.018.

Corzo, G., Solomatine, D., 2007. Baseflow separation techniques for modular artificial neural network modelling in flow forecasting. Hydrol. Sci. J. 52, 491–507 https://doi.org/10.1623/hysj.52.3.491.

Coulibaly, P., Anctil, F., Bobée, B., 2000. Daily reservoir inflow forecasting using artificial neural networks with stopped training approach. J. Hydrol. 230, 244–257 https://doi.org/10.1016/S0022-1694(00)00214-6.

De Vos, N.J., Rientjes, T.H.M., 2005. Constraints of artificial neural networks for rainfall–runoff modelling: trade-offs in hydrological state representation and model evaluation. Hydrol. Earth Syst. Sci. 9 (1/2), 111–126 https://doi.org/10.5194/hess-9-111-2005.

Deb, K., Pratap, A., Agarwal, S., Meyarivan, T., 2002. A fast and elitist multiobjective genetic algorithm: NSGA-II. IEEE Trans. Evol. Comput. 6, 182–197.

Dudhani, S., Sinha, A.K., Inamdar, S.S., 2006. Assessment of small hydropower potential using remote sensing data for sustainable development in India. Energy Policy 34, 3195–3205 https://doi.org/10.1016/j.enpol.2005.06.011.

Do Hoai, N., Udo, K., Mano, A., 2011. Downscaling global weather forecast outputs using ANN for flood prediction. J. Appl. Math.2011 https://doi.org/10.1155/2011/246286.

Eckhardt, K., 2005. How to construct recursive digital filters for baseflow separation. Hydrol. Process. 19, 507–515 https://doi.org/10.1002/hyp.5675.

Electricity Rates, 2018. Oklahoma City | Electricity Local, URL https://www.electricitylocal.com/states/oklahoma/oklahoma-city/, accessed 8.21.18).

Faber, B.A., Stedinger, J.R., 2001. Reservoir optimization using sampling SDP with ensemble streamflow prediction (ESP) forecasts. J. Hydrol. 249 (1–4), 113–133.

Fan, F.M., Schwanenberg, D., Alvarado, R., dos Reis, A.A., Collischonn, W., Naumman, S., 2016. Performance of deterministic and probabilistic hydrological forecasts for the short-term optimization of a tropical hydropower reservoir. Water Resour. Manag. 30 (10), 3609–3625.

Ficchì, A., Raso, L., Dorchies, D., Pianosi, F., Malaterre, P.O., Van Overloop, P.J., Jay-Allemand, M., 2015. Optimal operation of the multireservoir system in the Seine river basin using deterministic and ensemble forecasts. J. Water Resour. Plan. Manag. 142 (1), 05015005.

FIRO Overview, 2017. Center for Western Weather and Water Extremes. http://cw3e-web.ucsd.edu/firo/, (accessed 7.31.17).

Flint, L.E., Flint, A.L., 2012. Downscaling future climate scenarios to fine scales for hydrologic and ecological modeling and analysis. Ecological Processes 1 (1), 2 https://doi.org/10.1186/2192-1709-1-2.

Funahashi, K.I., 1989. On the approximate realization of continuous mappings by neural networks. Neural Network. 2 (3), 183–192 https://doi.org/10.1016/0893-6080(89)90003-8.

Funk, C., Peterson, P., Landsfeld, M., Pedreros, D., Verdin, J., Shukla, S., Husak, G., Rowland, J., Harrison, L., Hoell, A., Michaelsen, J., 2015. The climate hazards infrared precipitation with stations - a new environmental record for monitoring extremes. Scientific data 2, 150066.

Georgakakos, K.P., Graham, N.E., Georgakakos, A.P., Yao, H., 2007. Demonstrating integrated forecast and reservoir management (INFORM) for northern California in an operational environment. IAHS Publ. 313, 439.

Georgakakos, K.P., Graham, N.E., 2008. Potential benefits of seasonal inflow prediction uncertainty for reservoir release decisions. Journal of Applied Meteorology and Climatology 47 (5), 1297–1321.

Giuliani, M., Li, Y., Cominola, A., Denaro, S., Mason, E., Castelletti, A., 2016. A Matlab toolbox for designing Multi-Objective Optimal Operations of water reservoir systems. Environ. Model. Softw 85, 293–298 https://doi.org/10.1016/j.envsoft.2016.08.015.

Global Surface Summary of the Day, 2018. NOAA Data Catalog, URL https://data.noaa.gov/dataset/dataset/global-surface-summary-of-the-day-gsod, (accessed 1.30.18).

Govindaraju, R.S., Rao, A.R., 2000. Artificial Neural Networks in Hydrology. Kluwer Academic Publishers, Dordrecht, Netherlands.

Hamill, T.M., Bates, G.T., Whitaker, J.S., Murray, D.R., Fiorino, M., Galarneau Jr., T.J., Zhu, Y., Lapenta, W., 2013. NOAA's second-generation global medium-range ensemble reforecast data set. Bull. Am. Meteorol. Soc. 94, 1553–1565 https://doi.org/10.1175/BAMS-D-12-00014.1.

Humphrey, G.B., Maier, H.R., Wu, W., Mount, N.J., Dandy, G.C., Abrahart, R.J., Dawson, C.W., 2017. Improved validation framework and R-package for artificial neural network models. Environ. Model. Softw 92, 82–106 https://doi.org/10.1016/j.envsoft.2017.01.023.

Hutton, C.J., Kapelan, Z., 2015. A probabilistic methodology for quantifying, diagnosing and reducing model structural and predictive errors in short term water demand forecasting. Environ. Model. Softw 66, 87–97 https://doi.org/10.1016/j.envsoft.2014.12.021.

Jakeman, A.J., Letcher, R.A., Norton, J.P., 2006. Ten iterative steps in development and evaluation of environmental models. Environ. Model. Softw 21, 602–614 https://doi.org/10.1016/j.envsoft.2006.01.004.

Jain, A., Maier, H.R., Dandy, G.C., Sudheer, K.P., 2009. Rainfall runoff modelling using neural networks: state-Of-The-Art and future research needs. ISH J. Hydraul. Eng. 15, 52–74 https://doi.org/10.1080/09715010.2009.10514968.

Jordan, F.M., Boillat, J.-L., Schleiss, A.J., 2012. Optimization of the flood protection effect of a hydropower multi-reservoir system. Int. J. River Basin Manag. 10, 65–72 https://doi.org/10.1080/15715124.2011.650868.

Kişi, , 2005. Daily river flow forecasting using artificial neural networks and auto-regressive models. Turk. J. Eng. Environ. Sci. 29, 9–20.

Kişi, , 2007. Streamflow forecasting using different artificial neural network algorithms. J. Hydrol. Eng. 12 (5), 532–539.

Lee, S.-Y., Hamlet, A.F., Fitzgerald, C.J., Burges, S.J., 2009. Optimized flood control in the Columbia River basin for a global warming scenario. J. Water Resour. Plan. Manag. 135, 440–450 https://doi.org/10.1061/(ASCE)0733-9496(2009)135:6(440).

Li, X., 2005. Diversification and localization of energy systems for sustainable development and energy security. Energy Policy 33 (17), 2237–2243.

Lippmann, R.P., 1987. An introduction to computing with neural nets. IEEE ASSP Mag. 4–22.

Liu, H., 2010. On the Levenberg-Marquardt training method for feed-forward neural networks. Proceedings of 6th International Conference on Natural Computation 1, 456–460 https://doi.org/10.1109/ICNC.2010.5583151.

Lorrai, M., Sechi, G.M., 1995. Neural nets for modeling rainfall–runoff transformations. Water Resour. Manag. 9, 299–313.

Madsen, H., Richaud, B., Pedersen, C.B., Borden, C., 2009. A real-time inflow forecasting and reservoir optimization system for optimizing hydropower production. Waterpower XVI 1–12.

Maier, H.R., Dandy, G.C., 1996. The use of artificial neural networks for the prediction of water quality parameters. Water Resour. Res. 32 (4), 1013–1022 https://doi.org/10.1029/96WR03529.

Maier, H.R., Dandy, G.C., 2000. Neural networks for the prediction and forecasting of water resources variables: a review of modelling issues and applications. Environ. Model. Softw 15, 101–124 https://doi.org/10.1016/S1364-8152(99)00007-9.

Maier, H.R., Jain, A., Dandy, G.C., Sudheer, K.P., 2010. Methods used for the development of neural networks for the prediction of water resource variables in river systems: current status and future directions. Environ. Model. Softw 25, 891–909 https://doi.org/10.1016/j.envsoft.2010.02.003.

Mayne, D.Q., Rawlings, J.B., Rao, C.V., Scokaert, P.O., 2000. Constrained model predictive control: stability and optimality. Automatica 36 (6), 789–814.

Miao, Y., Chen, X., Hossain, F., 2016. Maximizing hydropower generation with observations and numerical modeling of the atmosphere. J. Hydrol. Eng. 21, 2516002 https://doi.org/10.1061/(ASCE)HE.1943-5584.0001405.

Monthly Charts for Grand Lake, 2018. O' the Cherokees, Pensacola Dm, URL http://www.swt-wc.usace.army.mil/PENScharts.html, (accessed 8.21.17).

Moré, J.J., 1978. The Levenberg-Marquardt algorithm: implementation and theory. Numer. Analysis 630, 105–116 https://doi.org/10.1007/BFb0067700.

Peel, M.C., Finlayson, B.L., McMahon, T.A., 2007. Updated world map of the Köppen-Geiger climate classification. Hydrol. Earth Syst. Sci. 11, 1633–1644.

Qi, Y.T., Luo, J.G., Wei, Y.X., Miao, Q.G., 2017. Maximizing hydropower generation in flood control operation using preference based multi-objective evolutionary algorithm. IOP Conf. Ser. Earth Environ. Sci. 86, https://doi.org/10.1088/1755-1315/86/1/012037.

Sikder, S., Ahmad, S.K., Hossain, F., Gebregiorgis, A., Lee, H., 2019. Case study: a rapid urban inundation forecasting technique based on quantitative precipitation forecast for Houston and harris county flood control district. J. Hydrol. Eng. https://doi.org/10.1061/(ASCE)HE.1943-5584.0001807.

Sudheer, K.P., Gosain, A.K., Ramasastri, K.S., 2002. A data-driven algorithm for constructing artificial neural network rainfall–runoff models. Hydrol. Proced. 16, 1325–1330 https://doi.org/10.1002/(ISSN)1099-1085.

Sudheer, K.P., Nayak, P.C., Ramasatri, K.S., 2003. Improving peak flow estimates in artificial neural network river flow models. Hydrol. Proced. 17, 677–686 https://doi.org/10.1002/hyp.5103.

Sun, Y., Wendi, D., Kim, D.E., Liong, S.Y., 2016. Application of artificial neural networks in groundwater table forecasting–a case study in a Singapore swamp forest. Hydrol. Earth Syst. Sci. 20 (4), 1405–1412.

Turner, S.W.D., Bennett, J.C., Robertson, D.E., Galelli, S., 2017. Complex relationship between seasonal streamflow forecast skill and value in reservoir operations. Hydrol. Earth Syst. Sci. 21 (9), 4841–4859.

Turner, S.W.D., Galelli, S., 2016. Water supply sensitivity to climate change: an R package for implementing reservoir storage analysis in global and regional impact studies. Environ. Model. Softw 76, 13–19.

Wei, C.C., 2016. Comparing single- and two-segment statistical models with a conceptual rainfall-runoff model for river streamflow prediction during typhoons. Environ. Model. Softw 85, 112–128 https://doi.org/10.1016/j.envsoft.2016.08.013.

Welsh, W.D., 2008. Water balance modelling in Bowen, Queensland, and the ten iterative steps in model development and evaluation. Environ. Model. Softw 23, 195–205 https://doi.org/10.1016/j.envsoft.2007.05.014.

Wilby, R.L., Wigley, T.M.L., 1997. Downscaling general circulation model output: a review of methods and limitations. Prog. Phys. Geogr. 21 (4), 530–548 https://doi.org/10.1177/030913339702100403.

Wu, C.L., Chau, K.W., Li, Y.S., 2009. Predicting monthly streamflow using data-driven models coupled with data-preprocessing techniques. Water Resour. Res. 45 (8) https://doi.org/10.1029/2007WR006737.

Wu, W., Dandy, G.C., Maier, H.R., 2014. Protocol for developing ANN models and its application to the assessment of the quality of the ANN model development process in drinking water quality modelling. Environ. Model. Softw 54, 108–127 https://doi.org/10.1016/j.envsoft.2013.12.016.

Xu, B., Zhong, P.A., Zambon, R.C., Zhao, Y., Yeh, W.W.G., 2015. Scenario tree reduction in stochastic programming with recourse for hydropower operations. Water Resour. Res. 51 (8), 6359–6380.

Yang, T., Gao, X., Sellars, S.L., Sorooshian, S., 2015. Improving the multi-objective evolutionary optimization algorithm for hydropower reservoir operations in the California Oroville-Thermalito complex. Environ. Model. Softw 69, 262–279 https://doi.org/10.1016/j.envsoft.2014.11.016.

Yazicigil, H., Houck, M.H., Toebes, G.H., 1983. Daily operation of a multipurpose reservoir system. Water Resour. Res. 19 (1), 1–13.

Zealand, C.M., Burn, D.H., Simonovic, S.P., 1999. Short term streamflow forecasting using artificial neural networks. J. Hydrol. 214 (1–4), 32–48 https://doi.org/10.1016/S0022-1694(98)00242-X.

Zemzami, M., Benaabidate, L., 2016. Improvement of artificial neural networks to predict daily streamflow in a semi-arid area. Hydrol. Sci. J. 61, 1801–1812 https://doi.org/10.1080/02626667.2015.1055271.

Zhang, G., Patuwo, B.E., Hu, M.Y., 1998. Forecasting with artificial neural networks: the state of the art. Int. J. Forecast. 14, 35–62 https://doi.org/10.1016/S0169-2070(97)00044-7.

Zhao, T., Cai, X., Yang, D., 2011. Effect of streamflow forecast uncertainty on real-time reservoir operation. Adv. Water Resour. 34 (4), 495–504 https://doi.org/10.1016/j.advwatres.2011.01.004.